Bis-Heteroleptic Cationic Iridium(III) Complexes Featuring Cyclometalating 2-Phenylbenzimidazole Ligands: A Combined Experimental and Theoretical Study

Emiliano Martìnez-Vollbert, Charles Ciambrone, William Lafargue-Dit-Hauret, Camille Latouche, Frédérique Loiseau, Pierre-Henri Lanoë

Bis-heteroleptic cationic iridium(III) complexes featuring cyclometallating 2-phenylbenzimidazole ligands: a combined experimental and theoretical study.

Emiliano Martìnez-Vollbert, Charles Ciambrone, William Lafargue-Dit-Hauret, Camille Latouche*, Frédérique Loiseau,* Pierre-Henri Lanoë*,

Authors

Emilliano Martínez-Vollbert, Charles Ciambrone, Frédérique Loiseau and Pierre-Henri Lanoë Univ. Grenoble Alpes, CNRS, DCM, 38000 Grenoble, France

Camille Latouche and William Lafargue-Dit-Hauret Université de Nantes, CNRS, Institut des Matériaux Jean Rouxel, IMN, F-44000 Nantes, France

ABSTRACT: In this report, we investigate a new family of cationic iridium(III) complexes featuring 2-phenylbenzimidazole cyclometallating ligand and 4,4'-dimethyl-2,2'-bipyridine ancillary ligand. Our benchmark complex $\mathbf{IrL^1_2}$ ($\mathbf{L^1}$ = 2-phenylbenzimidazole) displays similar emission properties than the archetypical complex 2,2'-dipyridyl-bis[2',4'-phenylpyridine]iridium(III) in deaerated CH_3CN (Φ = 0.20, λ_{em} = 584 nm ; Φ = 0.14, λ_{em} = 585 nm, respectively), but exhibits a higher photoluminescence quantum yield in deaerated CH_2Cl_2 (Φ = 0.32, λ_{em} = 566 nm; Φ = 0.20, λ_{em} = 595 nm, respectively), and especially lower non radiative constant (k_{nr} = 6.6 x 10^5 s^{-1} *vs* k_{nr} = 1.4 x 10^6 s^{-1}, respectively). As primary investigation, we explored the influence of the introduction of electron donating and electron withdrawing groups on the benzimidazole moiety and the synergetic effect of the substitution of the cyclometallating phenyl moiety in *para* position with same substituents. The emission energy displays very good correlation with the Hammett constants of the introduced substituents as well as with ΔE_{redox} values, which allow to ascribe the phosphorescence of these series to emanate mainly from a mixed metal/ligand to ligand charge transfer triplet excited state (^{3}M/LLCT*). Two complexes ($\mathbf{IrL^5_2}$ and $\mathbf{IrL^8_2}$) display a switch of the lowest triplet excited state from ^{3}M/LLCT* to ligand centered (^{3}LC*), from the less polar CH_2Cl_2 to the more polar CH_3CN. The observed results are supported by (TD)-DFT computations considering the vibrational contributions to the electronic transitions. Chromaticity diagrams based on the maximum emission wavelength of the recorded and simulated phosphorescence spectra demonstrate the strong interests of our complexes as emitting materials, together with the very good agreement between experimental and theoretical results.

Introduction

Phosphorescent iridium(III) complexes are a cornerstone of modern photochemistry since the beginning 21st century for a large number of applications such as emissive material in opto-electronics,[1–6] sensors and luminescent biological probes for confocal microscopy,[7–13] thanks to their high photoluminescence quantum efficiency, good electrochemical stability and reversibility, accessibility by reliable and robust methods. Finally, the judicious modification of the ligands allows the tunability of the emission color that spans from sky blue to near-infrared.[14,15,24–26,16–23] In addition to that, the triplet nature of their excited states made them suitable and efficient photosensitizers in photodynamic therapy (PDT) and in photocatalysis.[27,28]

The majority of the cationic iridium(III) complexes reported to date for lighting application, notably in Light Emitting Electrochemical Cells (LECs), derived from the archetypical complex: 2,2'-dipyridyl-bis[2',4'-phenylpyridine]iridium(III) ($[(ppy)_2Irbpy]^+$, with ppy = 2',4'-phenylpyridine and bpy = 2,2'-dipyridine, referred as $[(ppy)_2Irbpy]$ hereafter).[29–31] The highest occupied molecular orbital (HOMO) for $[(ppy)_2Irbpy]$ typically receives contributions from both an Ir(III) d-orbital

Figure 1: general structure of 2-phenylbenzimidazole base iridium complexes, R, R' and R'' represent the diverging point.

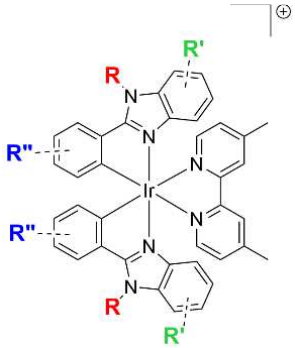

Scheme 1: Synthesis of the ligands and the corresponding complexes

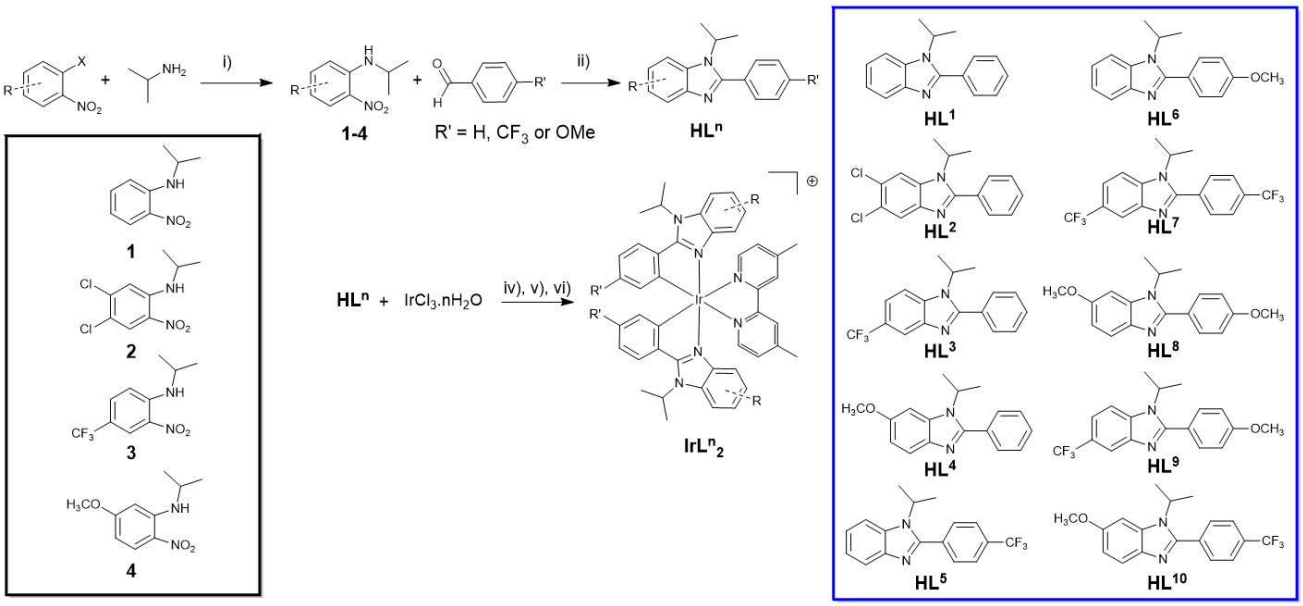

i) 60°C, Ar, DMSO; ii) $Na_2S_2O_5$, $HOCH_2CH_2OCH_2CH_3/H_2O$, reflux, overnight; iii) $HOCH_2CH_2OCH_2CH_3/H_2O$, reflux, overnight; iv) CH_2Cl_2/MeOH, reflux, overnight; v) KPF_6 (aq.) sat..

and from the π-system of the aryl rings of the cyclometallated ligands, while the lowest unoccupied molecular orbital (LUMO) has primarily π*-character localized on the ancillary ligand. The lowest lying excited state of this family of complexes is usually described as triplet metal-to-ligand charge transfer (^{3}MLCT*) admixed with ligand-to-ligand charge transfer (ancillary-based, ^{3}LL'CT*, L' = bpy or ancillary ligands) excited state, resulting in a broad emission profile.[3,14,29,32] Investigations of complexes derived from the archetypical [$(ppy)_2$Irbpy] complex reveal that the energy separation between the ^{3}MLCT* and the ^{3}LC* (ligand centered) is frequently small and in some cases the ^{3}LC* is the predominant emitting excited state.[3,14,22,29,32] The emission origin can be discriminated by the use of experimental method, such as steady state and time resolved emission spectroscopy and with the help of calculation.[14,30,33] For instance, the emission band shape will depend greatly on the nature of excited state, with broad featureless emission bands observed for ^{3}MLCT/^{3}LL'CT excited state phosphorescence while structured emission bands exhibiting vibronic progressions result from ^{3}MLCT/^{3}LC states. The nature of the emitting excited states will also affect radiative constant (k_r), which is typically of the order of 2 x 10^5 s^{-1} when the emission emanates from ^{3}MLCT/^{3}LL'CT excited state and lower in the case of the ^{3}LC phosphorescence.[14,33]

The excited state energies can be easily tuned by introducing electrodonating or electron withdrawing groups over the ligand by stabilizing and/or destabilizing the HOMO/LUMO levels.[24,29,30,34] For example, the archetypical [$(ppy)_2$Irbpy] displays an emission centered at 585 nm (Φ = 14% in deaerated CH_3CN),[3] whereas the introduction of methoxy groups on the cyclometallating phenyls destabilize the HOMO by electrodonating mesomeric effect and consequently the emission is bathochromically shifted. The resulting complexes series display emission centered in the range 600-730 nm (Φ = 15-0.2% in CH_3CN).[35]

As mentioned above, the majority of the reported cationic iridium(III) complexes are derived directly from the introduction of substituent on the 2-phenylpyridine ligand. In comparison, a fistful of iridium(III) complexes based on the use of 2-phenylbenzimidazole as cyclometallating ligand for neutral[36–44] and cationic[45–49] complexes are described. From a purely synthetic point of view, this ligand is presenting many advantages as scaffold for cyclometallating ligand, as it gives several divergence points (Figure 1). These latter can be independently modified and are (i) the introduction of alkyl or aryl on the secondary amine (R), (ii) on the phenyl ring (R'), (iii) on the benzimidazole ring (R"), and (iv) the synthesis does not require the use of palladium-catalyzed cross-coupling reactions.[50,51] Fine tuning of the emission properties can be achieved by the introduction of electron withdrawing/donating groups in (ii) and (iii) and the *bulkiness* of the final complex can be monitored, notably by the substitution in (i). Yet, the investigations toward this ligand have been limited to the modification of the phenyl,[36,38,49,39–44,47,48], the replacement of the benzimidazole by π-extended imidazole ring,[52] and the modification of the substitution of secondary amine with charge carrier units[37,42,45] or different alkyl chains or aryl groups, to name a few.[6,46,53]

For example, the iridium(III) complex featuring the cyclometallated ligand 1-methyl-2-phenylbenzimidazole and a phenanthroline as ancillary ligand has been reported to display an emission centered at 528 nm with a photoluminescence quantum yield (PLQY) of 51% in deaerated CH_2Cl_2.[45] The phosphorescence has been found to have more ^{3}MLCT* or ^{3}LLCT* character rather than ^{3}LC*.[45] The effect of chemical modifications of R' and R" of the 2-phenylbenzimidazole ligand (Figure 1)

has not been studied in iridium(III) cationic complexes. However, it has been demonstrated for neutral iridium(III) complexes with acetylacetonate as ancillary ligand, that the introduction of electron withdrawing/donating groups over the phenyl moiety allows to tune efficiently the emission. For example, the introduction of OMe groups in *meta* or *para* position of the phenyl, shifted the emission wavelength of the complex to 555 nm (Φ = 0.29) and 507 nm (Φ = 0.91), respectively, in comparison with the unsubstituted complex (520 nm, Φ = 0.64) in deaerated CH_2Cl_2.[43] Despite these promising results, deeper investigations have not been undertaken. Therefore, we report a series of cationic iridium(III) complexes featuring 2-phenylbenzimidazole cyclometallating ligands and 4,4'-dimethyl-2,2'-bipyridine ancillary ligand in which the electronic effect of chosen substituents over the benzimidazole moiety on the photophysical properties has been studied as well as the concomitant substitution of the benzimidazole moiety and the phenyl ring with antagonist or agonist substituents.

Results and discussion

Synthesis

The proligand synthesis was adapted from a two steps procedure using mild conditions. First, the isopropyl group was introduced using a previously reported procedure[51] which consists of an aromatic nucleophilic substitution of 2-fluoro/bromo-nitroarene by isopropylamine. The targeted nitroarenes were synthesized in high yields (79-97%). The desired 2-phenylbenzimidazole (**HL^n**) proligand, where H corresponds to the proton that will be removed by the cyclometallation reaction, was synthesized using an one pot procedure involving the *N*-isopropylnitroaniline that reacts with the suitable benzaldehyde in presence of a reducing agent ($Na_2S_2O_4$),[54] giving the desired new proligand from satisfactory to good yields (38-87%). The synthesis of the complexes was also performed using the well-known method of Watts[55] with 2-3 equivalents of cyclometallating ligand in a mixture of 2-ethoxyethanol/water refluxed in the presence of $IrCl_3.nH_2O$. The intermediate μ-Cl_2-(Ir**L^n**$_2$)$_2$ complex was directly engaged in the second step by the reaction with 4,4'-dimethyl-2-,2'-bipyridine (N^N) in a refluxing mixture of CH_2Cl_2/MeOH. The desired complex [(N^N)Ir**L^n**$_2$]$^+$ (referred as **IrL^n$_2$** hereafter) was obtained by precipitation with the addition of a saturated aqueous solution of potassium hexafluorophosphate and filtration. In some cases, the complex was further purified by flash chromatography column over silica gel. All the compounds have been characterized by the mean of ^{1}H, ^{13}C and ^{19}F NMR (all the spectra are in supporting information), mass spectroscopy and elemental analysis.

Structural characterizations

We succeeded to grow suitable crystals for X-ray diffraction for complexes **IrL^2$_2$**, **IrL^7$_2$** and **IrL^{10}$_2$**. Crystals have been obtained by slow vapor diffusion of either di(*iso*-propyl)ether or diethylether into a concentrated solution of complex in either 1,2-dichloroethane or dichloromethane, respectively and are shown in Figure 2. X-ray data have been gathered in table S1 and selected bond lengths and angles in table S2.

The three complexes crystallized in P 2_1/c, C 2/c, and P-1 for **IrL^2$_2$**, **IrL^7$_2$** and **IrL^{10}$_2$** respectively. The crystal structure of complex **IrL^7$_2$** displays two complexes per asymmetric unit, at the difference of the other two crystal structures where one

Figure 2: X-ray crystalline structures of complexes IrL^2$_2$, IrL^7$_2$ and IrL^{10}$_2$, hydrogens atoms and counterions have been omitted for clarity.

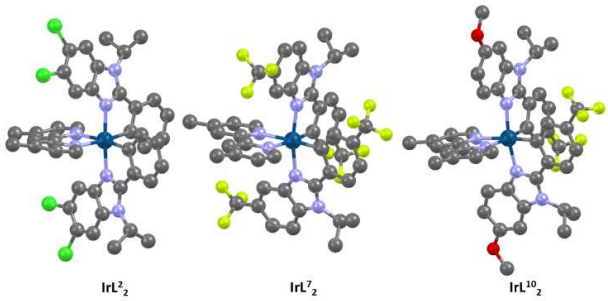

complex is found per asymmetric unit. As expected for centrosymmetric space groups, both enantiomers (Δ and Λ) are present in the lattice, whom are generated during the cyclometallation step leading to the dichloro-bridged dimers (Figure S1).[56] All the complexes display slightly distorted octahedral coordination environment and the nitrogen atoms from the cyclometallating ligand are in the expected *trans* position.[3,14,30,43,45,53,56,57] The C^Ir^N_{C^N} (N_{C^N} = coordinating nitrogen atom from the cyclometallating ligand) angles are roughly 79 ° and N_{C^N}^Ir^N_{C^N} are roughly 171°, both values being similar to the corresponding angles observed in the archetypical [(ppy)$_2$Irbpy] complex.[3] The Ir-C, Ir-N_{C^N} and Ir-N_{bpy} bond lengths are of the order of ~2.03 Å, ~2.05 Å and ~2.14 Å respectively, which are comparable with those of the archetypal (ppy)$_2$Irbpy$^+$ complex and of other related cationic Ir complexes.[3,14,30,43,45,53,56,57] The Ir-N_{bpy} distances are longer than the Ir-N_{C^N} due to the so called *trans* effect which is a consequence of the strong σ-donating ability of the cyclometallating carbon atoms.[3] The cyclometallation induced an obvious rigidification of the phenylbenzimidazole ligand, with the loss of free rotation around the C-C bond between the phenyl and the benzimidazole. An unforeseen consequence is the restriction of the motion of the *iso*-propyl groups. Indeed, the average distance observed between the protons H5 and H14 (proton in *ortho* of the benzimidazole-phenyl bond and the proton of the methylene of the isopropyl group, respectively) in the X-ray structure of the three complex is ~1.95 Å, which is below the sum of the Van der Waals radii (VdW). The spatial proximity remains in solution as in ^{1}H NMR spectroscopy the heptuplet corresponding to this proton is down-field shifted (average of 0.8 ppm, table S3 and ^{1}H NMR spectra in supporting material) upon cyclometallation, with respect to the corresponding proligand.

A deeper look to the complexes structure reveals that cyclometallating ligands display dihedral angles between the imidazole ring and the arene, from 1(1) ° to 11.5(6) °, and so do the bipyridine ancillary ligand, from 3.4(6) ° to 13.0(9) °. The archetypal [(ppy)$_2$Irbpy] complex displays also distortions in the ligands, but somewhat smaller between 1.5(6) ° and 6.0(5) ° for the cyclometallating ligands and 1.4(6) ° for the N^N ancillary ligand, which are closer to the expected planarity.[3] On an other hand, such distortions are encountered in other 2-phenylbenzimidazole based iridium cationic and neutral complexes, regardless of the presence of alkyl or aryl group on the nitrogen atom (namely methyl or phenyl groups).[43,45,53,57] For

Figure 3: X-ray crystalline structure of complex IrL^2_2, hydrogens atoms and PF_6 anions have been omitted for clarity.

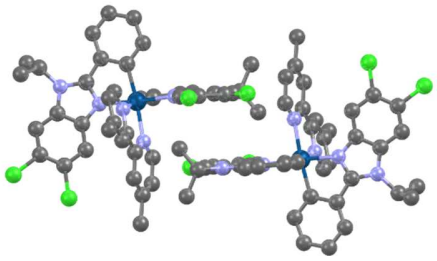

example, dihedral angles up to 14.4 ° and 11.3 °, for the N-methyl substituted 2-phenylbenzimidazole and bipyridine respectively, have been encountered.[53]

The solid-state structure of complex $\mathbf{IrL^2_2}$ displays interesting supramolecular architecture. First, the 2-phenylbenzimidazole ligands are not equivalent in the crystal structure, as they display different dihedral angles of 2.0(1) ° and 8.4(9) °. In stark contrast, the benzimidazole moieties beared by adjacent complexes involved in the supramolecular arrangement (*vide infra*) are almost parallel with centroïd-centroïd distances ~3.960 Å and ~4.081 Å (Figure 3). The bpy ligand displays the larger dihedral angle of 13.0 (0) ° of the three complexes, which may result from chlorine-arene interactions. Indeed, the average $Cl\cdots C_{py}$ distance is 3.26 Å (table S4 and figure S2) which is below the sum of the VdW radii (3.45 Å). In addition, the C-Cl bonds lengths of the involved chlorine atoms are 1.746(7) Å and 1.740(7) Å, which are longer than the other C-Cl bond lengths (i.e. 1.730(8) Å and 1.731(8) Å). The slight elongation can be attributed to the interactions between the halogen atoms and the π-system from the pyridines, such interactions have been previously described, for example, in cocrystals constructed by 1,4-diiodotetrafluorobenzene and polyaromatic hydrocarbons.[58] The observed interactions are consistent with the presence of halogen bonding between the chlorine atoms and a π-system of the bipyridine ligand. Indeed, halogen atoms act as electron-deficient sites (the so called σ-hole is positioned at the opposite of the C-X bond) and can interact with an electron rich partner.[59,§] It is worth noting that the presence of halogen bonding is scarcely observed in octahedral cyclometallated iridium(III) complexes.[60] Here, the halogen bonds are established in a supramolecular architecture that results in the building of supramolecular polymers in the lattice (figure S2).

A close look to the crystal structure of $\mathbf{IrL^7_2}$ reveals numerous electrostatic interactions between fluorine atoms and hydrogen and carbon atoms, with distances that are less than the sum of the VdW 2.56 Å and 3.17 Å respectively. For example, the two complexes of the asymmetric unit display interactions between fluorine atoms and carbon atoms (F6-C76 = 2.957(8) Å and F3-C7 = 3.152(7) Å). These interactions are also present between asymmetric unit complexes. Indeed, electrostatic bonding can be observed between fluorine atoms of the CF_3 group and the hydrogen atoms form the methyl group of the dmp (F12-H48C = 2.53 Å). These interactions (see table S4) lead to a supramolecular organization within the lattice.

The analysis of the crystal packing of complex $\mathbf{IrL^{10}_2}$ reveals the presence of hydrogens bonding with an electrostatic nature between hydrogen atoms (H16, H22, H23 and H24) and oxygen (O1), carbon (C11) and fluorine (F1B and F2B) atoms respectively.[61] In each case, the observed distances are below the sum of the VdW radii H16-F1B = 2.57 Å, H22-C112.854 Å, H23-O1 = 2.6 Å and H24-F2B = 2.48 Å.

Electrochemical properties

In order to assess the reversibility and the energies of the first reduction and oxidation waves, cyclic voltammetry (CV) was carried out in deaerated CH_3CN. The CVs were performed using vitreous carbon working electrode, *n*-NBu_4PF_6 (0.1 M) supporting electrolyte and $Ag/AgNO_3$ (0.01 M) as reference electrode and with a scan rate of 100 $mV.s^{-1}$. The redox potentials are given versus the reference electrode. CV traces are shown in Figure 4 and values are gathered in Table 2.

Figure 4: Cyclic Voltamperometry traces of the complexes' series in CH_3CN (10^{-3} M) solution, reported versus $AgNO_3$ (10^{-2} M). Scan rates were at 100 $mV.s^{-1}$ and are in the positive scan direction.

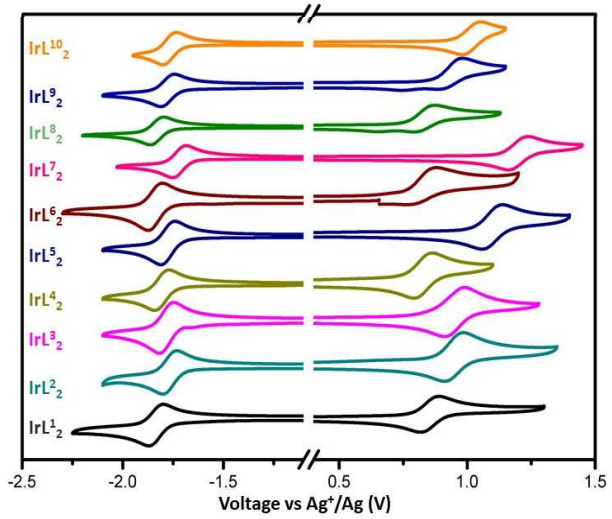

§ In addition, halogen atoms can act as electron donors orthogonally to the C-X bond with an electron deficient partner such as a hydrogen. For deeper discussion readers are invited to consult ref 58 and the references inside.

Figure 5: Absorption spectra in CH_3CN at 298 K.

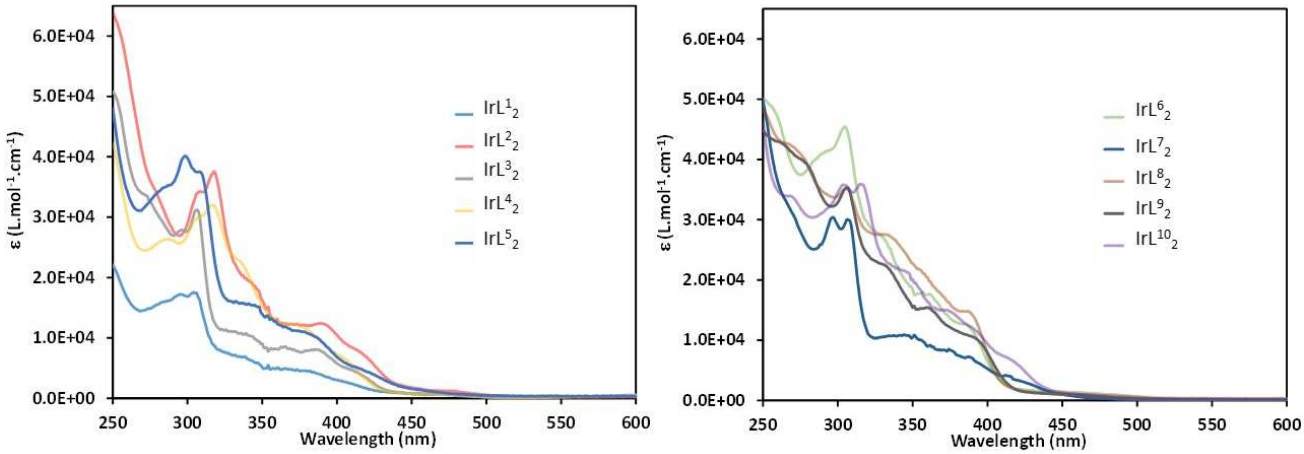

The complexes display fully reversible reduction waves in the range -1.87 – -1.75 V. The reduction can be ascribed to the one electron reduction of the N^N ancillary ligand, which is supported by previous works on similar iridium complexes.[30,62,63] The reduction potentials are slightly sensitive to the nature of the substituents. Intriguingly, the incorporation of electrowithdrawing group into the N^C ligand framework has quite a strong effect on E_{red}, making it less negative. For example, when a CF_3 group is present on the *para* position of the phenyl (**IrL$^5_2$**), the E_{red} is less negative by +60 mV and when two chlorine atoms (**IrL$^2_2$**) are on the benzimidazole moiety E_{red} increases by +70 mV, with respect to the complex bearing no substituent (E_{red} = -1.87 V). In addition, the presence of two withdrawing groups on both the benzimidazole and the phenyl moieties (**IrL$^7_2$**) have a synergetic effect. Indeed, the E_{red} displays the largest shift of the series with a +170 mV increase. Hence, even if the LUMO is predominantly localized on the N^N ligand, in agreement with theoretical calculation and previous studies, the electron withdrawing groups decrease the electronic density of this orbital.[62,64] On another hand, the presence of electron donating groups by mesomeric effect (OCH_3, **IrL$^{4,8\text{-}10}_2$**) has almost no influence on the reduction potential.

In the anodic region, all the complexes display a reversible wave within the range 0.86 V – 1.23 V, which can be attributed to the oxidation of the metal core from Ir^{III} to Ir^{IV}, in agreement with theoretical studies and previous works.[30,62,63] In the three complexes **IrL$^8_2$**, **IrL$^9_2$** and **IrL$^6_2$**, the introduction of methoxy groups makes the single oxidation event irreversible. The oxidation potential of the iridium core is sensitive to the nature of the substituent present on the C^N ligand and especially to the presence of electrowithdrawing groups. The introduction of chlorine atoms on the benzimidazole moiety (**IrL$^2_2$**) renders the E_{ox} more positive (+ 100 mV), with respect to the complex bearing no substituents (E_{ox} = 0.89 V). On the other hand, the presence of a methoxy on this part of the cyclometallating ligand has a lower impact. These groups induce a small change in the E_{ox} (- 30 mV), which can be attributed to the electronic ability (+M and -I) of these two groups. Substitution on *para* position of the phenyl by a CF_3 group (**IrL$^5_2$**) affects dramatically E_{ox}, with an anodic shift of +150 mV with respect to complex **IrL$^1_2$** (E_{ox} = 0.89 V). In contrast, the introduction of the electrodonating methoxy group in same position has less impact, hence the E_{ox} are shifted with a maximum of +30 mV. The introduction of two methoxy groups on both the benzimidazole and the phenyl moieties results in a synergetic effect on the E_{ox}. The CF_3 groups on both side of the cyclometallating ligand have a synergetic effect as complex **IrL$^7_2$** displays the highest E_{ox} of the series.

In conclusion, the redox potentials reflect the electronic influence of the substituents introduced on the cyclometallating ligand, even if the presence of electrodonating groups either on the benzimidazole moiety or the *para* position of the phenyl induces almost no change. In contrast, the concomitant presence of CF_3 in *para* position of the phenyl and OMe on the benzimidazole moiety allows to moderate the influence of the electrowithdrawing groups, and especially the E_{ox}. Complex **IrL$^{10}_2$** displays an E_{ox} intermediate between those of complexes **IrL$^3_2$** and **IrL$^7_2$**.

UV-Vis absorption

The room-temperature electronic absorption spectra have been recorded in diluted CH_2Cl_2 and CH_3CN solutions and are reported in Figure 5, Figure S3, Table 1 and Table 2 (individual spectra are to be found in SI. The complexes display similar absorption spectra, that could be divided in three main domains as expected for cationic cyclometallated iridium(III) complexes.[14,30] Below 330 nm, intense and moderately intense transitions are observed, that are usually ascribed to spin-allowed π-π^* transition (^{1}LC) from the cyclometallating ligand and the ancillary ligand. From 330 nm to 425 nm, weaker absorption bands are observed and they are attributed to spin-allowed charge transfer transition, from the metal to the ligand (^{1}MLCT) and from the cyclometallating ligand to the ancillary ligand (^{1}LLCT).[14] The weak tails observed above 420 nm (Figure S4) are due to direct spin-forbidden transitions leading to ^{3}MLCT and ^{3}LLCT excited states, permitted by the high spin-orbit coupling constant (ζ = 3909 cm^{-1}) of the iridium core.[14] The latter increases significantly the intersystem crossing to the triplet excited states.[14,30]

Figure 6: Emission spectra in CH_3CN at 298 K.

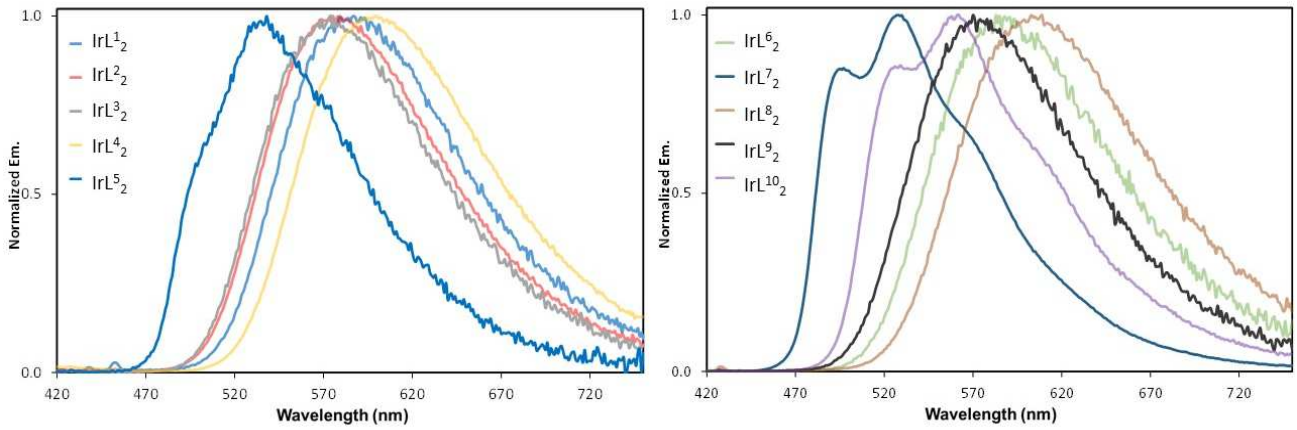

Emission spectroscopy

Emission spectra have been recorded in diluted CH_2Cl_2 and CH_3CN solutions, under air equilibrated and deaerated conditions. The spectra and data are gathered in Figure 6 (individual spectra are to be found in SI), Table 1 and Table 2. The CIE diagram obtained at λ^{em}_{max} in CH_2Cl_2 is presented in Figure 10 top. The complexes display relatively similar broad emission spectra, to the exception of complexes bearing CF_3 (**IrL^3$_2$**, **IrL^5$_2$**, **IrL^7$_2$** and **IrL^9$_2$**) groups whom emissions are more structured. As expected, the maximum wavelength depends on the nature of the substituents present on the cyclometallating ligand. For example, the emission of the complex bearing two chlorine atoms (**IrL^2$_2$**) over the benzimidazole ring displays a hypsochromic shift with respect to **IrL^1$_2$**. On the other hand, a bathochromic shift is observed with the emission displayed by **IrL^4$_2$**, with comparison with complex **IrL^1$_2$**.

The complexes display high photoluminescence quantum yields (PLQY) under argon ranging from 0.13 up to 0.65 and are air sensitive (*vide infra*). It is worth noting that the PLQYs follow energy gap law (Figure S8) based on Fermi's golden rule, which associates the increase of k_{nr} at small Franck-Condon energy with increased vibrational wavefunction overlap.[65]

Cyclometallated Ir(III) complexes are known to be good sensitizers for singlet oxygen and gained attention in phototherapy dynamic.[28,66–68] The O_2-quenching constants ($k_Q(O_2)$) have been estimated for the series and are somewhat high, ranging from 6.3 x 10^8 $M^{-1}.s^{-1}$ to 3.5 x 10^9 $M^{-1}.s^{-1}$ in CH_2Cl_2 and 2.3 x 10^8 $M^{-1}.s^{-1}$ to 2.1 x 10^9 $M^{-1}.s^{-1}$ in CH_3CN (with $[O_2]$ = 2.2 mM and 9.1 mM, in CH_2Cl_2 and CH_3CN respectively[69]). These results are in line with reported values and confirm the trend that monocationic Ir(III) complexes seem to be less sensitive to molecular oxygen than their neutral counterparts. For example in air equilibrated CH_3CN solution, the complex $(btp)_2Ir(acac)$ (btp = 2-pyridylbenzothiazole, acac = acetylacetonate) displays a $k_Q(O_2)$ of 6.3 x 10^9 $M^{-1}.s^{-1}$, whereas the monocationic complex $(btp)_2Ir(phenNH_2)$ ($phenNH_2$ = 1,10-phenanthrolin-5-amine) displays a $k_Q(O_2)$ of 2.4 x 10^9 $M^{-1}.s^{-1}$.[28,66,67]

To have a better insight into the photophysical properties of the complexes, the benchmark of the series, complex **IrL^1$_2$**, can be compared with the archetypical complex $[(ppy)_2Irbpy]$. In deaerated CH_3CN, both complexes display a broad emission centered at 584 nm and 585 nm, respectively, and the PLQY are similar Φ = 0.20 and Φ = 0.14, respectively. The luminescence decays are also very close to each other, with 0.76 µs and 0.43 µs, respectively for **IrL^1$_2$** and $[(ppy)_2Irbpy]$.[3,30,70] The radiative and non-radiative constants are, thus, of the same order of magnitude (**IrL^1$_2$**, k_r = 2.7 x 10^5 s^{-1} and k_{nr} = 1.10 10^6 s^{-1} ; $[(ppy)_2Irbpy]^+$, k_r = 3.3 x 10^5 s^{-1} and k_{nr} = 1.99 x 10^6 s^{-1}). The two complexes have very similar photophysical properties at least in CH_3CN. However, beside the same emission shapes displayed by the two complexes, they have distinct behaviour in deaerated CH_2Cl_2, $[(ppy)_2Irbpy]$ exhibits a bathochromic shift compared to the emission in CH_3CN (λ_{em} = 595 nm)[3,30,70], whereas complex **IrL^1$_2$** 's emission is centered at 566 nm. PLQY of the benchmark **IrL^1$_2$** complex of the series is significantly higher than the one of $[(ppy)_2Irbpy]$, with Φ = 0.32 compared to Φ = 0.20.[3,30,70] Nonetheless, the radiative constants are nearly identical for both complexes k_r ~ 3.0 x 10^5 s^{-1}, but the nonradiative constant is significantly lower for **IrL^1$_2$** with k_{nr} = 6.6 x 10^5 s^{-1}, than for the archetypical $[(ppy)_2Irbpy]$ complex, k_{nr} = 1.4 x 10^6 s^{-1}.[3,30,70] Such results steered us to investigate more deeply this new family of cationic iridium complexes based on the scaffold 2-phenylbenzimidazole cyclometallating ligand. First, a modification of the benzimidazole ring was considered, through the introduction of electro-withdrawing and electron-donor groups.

The introduction of electron withdrawing groups over the benzimidazole ring yields the expected effect to induce a hypsochromic shift of the emission wavelength. For example, the complex **IrL^3$_2$** displays an emission centered at 544 nm with PLQY of 0.53 and a decay of 1.24 µs, in degassed CH_2Cl_2. Thus, the k_r (4.3 x 10^5 s^{-1}) is faster than in the benchmark **IrL^1$_2$** complex to the contrary of the k_{nr} (3.8 x 10^5 s^{-1}). The complex $[(3\text{-}CF_3ppy)Irdmp]^+$ also displays a hypsochromic shift in emission (λ_{em} = 515 nm, Φ = 0.67, τ = 1.20 µs, in degassed CH_2Cl_2) in comparison with the archetypical $[(ppy)_2Irbpy]$ complex.[71] However, the latter shift is stronger than the one observed in **IrL^3$_2$** and it could be related to the fact that the electron withdrawing group is far from the metal core and its influence over the electron density is less than in the case of $[(3\text{-}CF_3ppy)Irdmp]^+$ where only three bonds separate the CF_3 group

from the Ir(III). In addition to that, the HOMO is mainly localized over the metal core and the phenyls and, hence, the influence is stronger.[29,30] In degassed CH_3CN, the emission of $\mathbf{IrL^3_2}$ is significantly bathochromically shifted (λ_{em} = 589 nm, 140 cm^{-1}) and the PLQY drops to 0.27 and so does the decay to 0.91 µs. The reduction of the PLQY and lifetime are illustrated by the higher k_{nr} (8.0 x 10^5 s^{-1}) value in this solvent than the k_r (3.5 x 10^5 s^{-1}). The somewhat strong sensitivity to the solvent polarity could be assigned to a stronger contribution of the ^{3}MLCT* in the emitting excited states for this compound in comparison with $\mathbf{IrL^1_2}$.

Corollary, the introduction of electron donating groups over the benzimidazole has an antagonist effect. Indeed, the emission spectrum displayed by complex $\mathbf{IrL^4_2}$ is bathochromatically shifted with respect to $\mathbf{IrL^1_2}$, with a broad emission centered at 586 nm with PLQY of 0.34 and a decay of 0.95 µs, in deaerated CH_2Cl_2. The radiative and non-radiative constants are 3.6 x 10^5 s^{-1} and 7.0 x 10^5 s^{-1}, respectively. Despite the redshifted emission, the photophysical properties are slightly higher than the benchmark complex ($\mathbf{IrL^1_2}$, k_r = 2.7 x 10^5 s^{-1} and k_{nr} = 1.1 10^6 s^{-1}). In deaerated CH_3CN, the emission spectrum displays a positive solvatochromism (400 cm^{-1}) with a broad emission centered at 600 nm and a shortened decay of 0.16 µs in comparison with the emission in CH_2Cl_2. The PLQY is seriously impacted by the solvent change and drops to 0.02, which is illustrated by a greater k_{nr} (2.5 x 10^6 s^{-1}) value than k_r (13.1 x 10^5 s^{-1}). The positive solvatochromism along with the broad shape of the emission is consistent with an excited state with a predominant contribution of the ^{3}MLCT*.

Secondly, the influence of two substituents (-CF_3 and -OMe) in the *para* position of the phenyl moiety has been investigated.

Complex $\mathbf{IrL^5_2}$ displays a broad emission centered at 530 nm (Φ = 0.65, τ = 1.16 µs) in deaerated CH_2Cl_2. In comparison with complex $\mathbf{IrL^3_2}$ (Φ = 0.53, λ_{em} =544 nm, τ = 1.24 µs), the effect of the electron withdrawing group is more important when it is positioned on the phenyl than on the benzimidazole ring, as the substituent is closer to the metal core and as the HOMO is predominantly localized over the Ir(III) and the phenyls.[14,29,30] The radiative and non-radiative constants, in addition to the broadness of the emission, suggest that the excited state is predominantly ^{3}MLCT* in nature.[14] However, switching to a more polar solvent (i.e. CH_3CN), the emission displayed by the complex is different with apparition of structuration that shows a *pseudo* vibronic progression of the order of 1400 cm^{-1}. In addition, k_r drops to 8.9 x 10^4 s^{-1} which is a strong indication of ^{3}LC* emission.[14,72] Complex $\mathbf{IrL^5_2}$ is a rare example of switching between excited states (i.e. ^{3}MLCT* to ^{3}LC*) induced by solvent polarity.[73] Counter intuitively, the increase of polarity stabilized the energy level of the ^{3}LC* more efficiently than the ^{3}MLCT* energy level. Nonetheless, as in the large majority of Ir(III) complexes, the origin of the emitting excited state is scarcely of a pure nature (i.e. ^{3}MLCT*, ^{3}LC*, ^{3}LLCT*), but resides in a subtle mixture of the different accessible excited states.[14,30,33] Indeed, the low temperature emission spectrum of the complex (77 K in butyronitrile) is strongly blue shifted with a more pronounced vibronic progression of the emission shape. Such a behavior is typical of an emission with a contribution of ^{3}MLCT*.[14,74]

The introduction of an electron-donating group in *para* position of the phenyl ring has the expected effect of inducing a bathochromic shift of the emission displayed by the complex $\mathbf{IrL^6_2}$, with respect to complex $\mathbf{IrL^1_2}$. The emission spectrum is broad and centered at 570 nm (Φ = 0.40, τ = 1.16 µs) in deaerated CH_2Cl_2 and, when compared to the emission displayed by complex $\mathbf{IrL^4_2}$, it appears that the influence of the methoxy group in *para* position of the phenyl has a lower impact than when positioned on the benzimidazole moiety, which is in line with the observations in electrochemistry (*vide supra*). The emission in deaerated CH_3CN displays a bathochromic shift with respect to the emission in the less polar CH_2Cl_2 and the PLQY drops to 0.09 with a decay of 0.43 µs. At first glance, the luminescence properties are lower than those of the complexes $[(4\text{-OMeph-5-Mepy})_2Ir(N\text{^}N)]^+$ (with N^N = 4,4'-di*tert*-butyl-2,2'-bipyridine and 4-OMeph-5-Mepy = 2-(4-methoxyphenyl)-5-methylpyridine) which display a broad emission centered at 585 nm (Φ = 0.15, τ = 0.39 µs).[35] A close look to the k_r and k_{nr} indicates that if k_r is slightly superior for the complex $[(4\text{-OMeph-5-Mepy})_2Ir(N\text{^}N)]^+$ (k_r = 3.9 x 10^5 s^{-1} *vs* k_r = 3.0 x 10^5 s^{-1}), k_{nr} constant is slightly advantageous (k_{nr} =2.2 x 10^6 s^{-1} *vs* k_{nr} = 8.0 x 10^5 s^{-1}) for the imidazole derivatives.

Finally, we investigated the simultaneous substitution of both the benzimidazole ring and the phenyl moiety. The introduction of electron withdrawing/donating on both the sides of the cyclometallating ligand demonstrates to have synergic effect on the emission, as it has been observed in voltamperometry. Two methoxy groups ($\mathbf{IrL^8_2}$) lead to a bathochromic shift of the emission (585 nm in CH_2Cl_2 and 603 nm in CH_3CN). The radiative rate is of the order of 3.6 x 10^5 s^{-1}, which is in favor of an emissive excited state with an important contribution of ^{3}MLCT*. It is worth noting that the introduction of electron withdrawing groups (CF_3) has for consequence the hypsochromic shift of the emission wavelength, and $\mathbf{IrL^7_2}$ displays a structured emission in both the studied solvents with a vibronic progression of ~1300 cm^{-1} (CH_2Cl_2 and CH_3CN). In addition, the radiative rate in both solvents is of the order of 2 x 10^5 s^{-1}, therefore the emitting excited state has a strong contribution of the ^{3}LC*.

The introduction of antagonist substituents (i.e. CF_3 and OMe) on the benzimidazole and the phenyl moieties has the excepted effect of mitigating the influence of these groups on the photophysical properties. That is to say, as above mentioned, the CF_3 groups have a stronger effect than OMe groups and the introduction of the latter attenuates the induced hypsochromic shift on the emission spectra of complexes $\mathbf{IrL^9_2}$ and $\mathbf{IrL^{10}_2}$, in comparison with complexes $\mathbf{IrL^3_2}$and $\mathbf{IrL^5_2}$ respectively.

To conclude on the photophysical studies, the nature of the emission can be ascribed to phosphorescence according to (i) Stoke's shifts, (ii) oxygen sensitivity, (iii) long decays of the emission. The emitting excited state has a large contribution of the ^{3}M/LLCT*, in accordance with (i) emission shape, (ii) the positive solvatochromism,[75] (iii) the rigidochromism effect observed at 77 K[74], (iv) the radiative constants that are above 2.0 x 10^5 s^{-1},[14] regardless the solvent, (v) the correlation between the emission energy and the ΔE_{redox} (Figure S9) (that illustrates that the emitting levels of this series of complexes have a predominant ^{3}CT*),[76] and (vi) the TD-DFT calculations, to the exception of four complexes $\mathbf{IrL^5_2}$, $\mathbf{IrL^7_2}$, $\mathbf{IrL^8_2}$ and $\mathbf{IrL^{10}_2}$ and these complexes could be divided in two subgroups. Complexes $\mathbf{IrL^7_2}$ and $\mathbf{IrL^{10}_2}$ have a strong contribution of the ^{3}LC* in the

Figure 7: Simulation of TD-DFT absorption spectra for Ir(III) complexes.

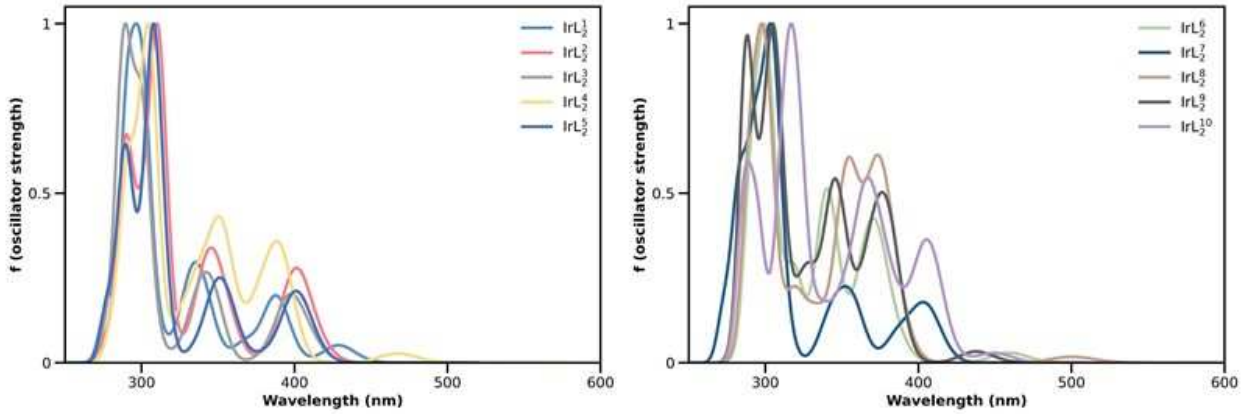

emitting excited state, which is illustrated by the vibronic structure of emission in both solvents. A second set of complexes, namely **IrL$^5_2$** and **IrL$^8_2$** display a somewhat uncommon behavior with increasing the solvent polarity, by switching the predominant contribution from ^{3}MLCT* in CH_2Cl_2 to ^{3}LC*, with regard to the decrease of the radiative rate and the structuration of the emission in CH_3CN (*vide supra*). Finally, the introduction of substituents on the benzimidazole or the phenyl, and on both the arenes, enables the tuning of the molecular orbital energies, both the HOMO and LUMO levels as illustrated by the correlation of the emission energy with the Hammett parameters (Figure S10), and thus the emission wavelength in accordance with the observation in the cyclic voltamperometry (*vide sup*ra) and the introduction of antagonist groups (i.e. OMe and CF_3) tempered their electronic effect.

Theoretical investigation

To gain a deeper insight into the nature of the electronic structure and transitions occurring in such complexes, *ab initio* calculations were performed on all species. Density Functional Theory (DFT) simulations have been performed using the Gaussian16 package.[77] Based on previous theoretical investigations conducted by some of us,[78–81] we considered the B3PW91 functional[82–84] in addition to the LanL2Dz basis set, which includes a pseudopotential to describe core electrons for large atoms together with polarization functions on C (d; 0.587), N (d; 0.736), O (d; 0.961), F (d; 1.577) Cl (d; 0.75) and Ir (f; 0.938).[85–89] The Polarizable Continuum Model (PCM)[90,91] was used to take into account solvent effects (CH_2Cl_2). For computational savings, the -OMe and -NiPr fragments were replaced by -OH and -NH groups. Geometry relaxations of the singlet (ground state) and triplet (excited state) states were performed and carefully checked by the calculation of the vibrational frequencies. The general Adiabatic Hessian approach (AH)[92] was considered for estimating vibrational contributions into the computation of emission spectra. Post-treatments were done using the Gaussview and VMS packages.[93–95] Horseshoe plots were realized using an in house Python code.

First, geometry optimizations were conducted for the ground singlet state and compared to the experimental crystallographic data. We found that our relaxed structures are in good agreement with the experimental ones, as evidenced, for example, by the average of Ir-C, Ir-N_{C^N} and Ir-N_{bpy} bonds of 2.02 Å (exp. ~2.03 Å), 2.06 (exp. ~2.05 Å) and 2.15 Å (exp. ~2.14 Å), respectively (more details for each complex are given in Supporting Information). Such results give us confidence for complementary analyzes. Based on the fully relaxed geometries, TD-DFT calculations were performed to simulate the excitation spectra for transitions above 330 nm. In the following, since the trend is identical for all complexes, we only focus the discussion on **IrL$^1_2$**. Figure 8 shows the molecular orbitals (MO) diagram of the **IrL$^1_2$** complex, the other MOs diagrams are provided in SI. One may notice that the highest occupied MOs possess a strong iridium *d* character, while the lowest unoccupied MOs are mainly localized on either the cyclometallating or the ancillary ligands. For all complexes the band gap is quite large (> 2.90 eV) leading to a strong thermodynamic stability.

Figure 8: Frontier MOs of IrL1$_2$ at the singlet state (isovalue level= 0.05).

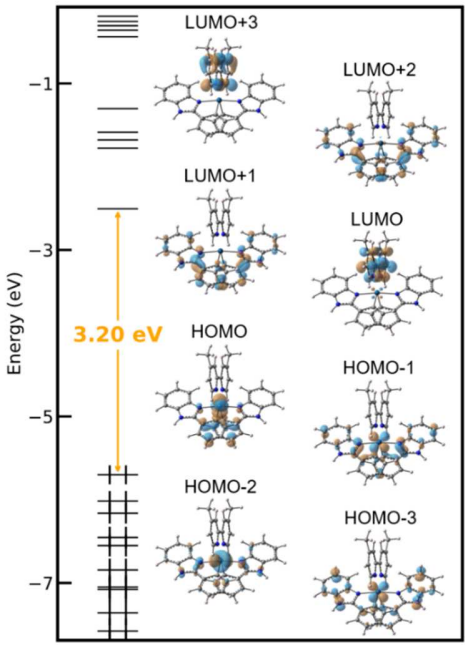

Table 1: Photophysical properties in dichloromethane and in glassy solution at 77 k.

Complex	absorption λ [nm] (ε × 10^3 [M^{-1} cm^{-1}])	Photoluminescence (278 K)[a,b] in CH_2Cl_2						Photoluminescence (77 K)[c]	
		λ [nm]	Φ (air)	τ [µs] (air)	k_r x 10^5 [s^{-1}]	Σk_{nr} x 10^5 [s^{-1}]	$k_Q[O_2]$[d] x 10^9 [$M.s^{-1}$]	λ [nm]	τ [µs]
IrL^1_2	285 (19.6), 297 (20.1), 307 (20.3), 334 (8.2), 383 (5.3), 407 (2.7), 470 (0.6)	566	0.32 (0.08)	1.03 (0.19)	3.1	6.6	1.2	512*, 546	19.67
IrL^2_2	278 (34.8), 308 (34.3), 319 (36.9), 346 (18.1), 392 (12.2), 423 (6.0), 479 (1,2)	557	0.46 (0.07)	1.32 (0.26)	3.5	4.1	2.0	514*, 539	13.37
IrL^3_2	274 (32.9), 296 (27.9), 306 (31.2), 338 (10.5), 364 (8.4), 387 (8.0), 411 (4.6), 469 (0.6)	554	0.53 (0.10)	1.24 (0.22)	4.3	3.8	1.7	507*, 538	12.51
IrL^4_2	288 (30.5), 309 (31.7), 320 (34.6), 336 (25.5), 378 (13.2), 405 (8.1), 474 (0.8)	586	0.34 (0.11)	0.95 (0.23)	3.6	7.0	1.0	527*, 558	19.61
IrL^5_2	285 (28.8), 299 (31.0), 310 (29.0), 345 (12.4), 383 (9.3), 414(4.5), 467 (1.2)	530	0.65 (0.16)	1.59 (0.49)	4.1	2.2	0.9	489*, 528, 571	4.45
IrL^6_2	289 (36.6), 304 (38.6), 331 (23.9), 362 (16.0), 387 (11.4), 468 (0.8)	570	0.40 (0.09)	1.16 (0.28)	3.4	5.2	1.3	525*, 557	20.68
IrL^7_2	271 (33.0), 291 (31.6), 306 (31.3), 344 (11.7), 390 (79.7), 418 (4.5)	493, 526*, 575	0.54 (0.12)	2.40 (0.57)	2.2	1.9	0.6	484*, 521, 564, 615	3.88
IrL^8_2	272 (30.4), 305 (24.1), 339 (19.0), 388 (10.8), 498 (0.5)	585	0.13 (0.03)	0.57 (0.24)	3.0	20.2	3.5	527*, 558	18.72
IrL^9_2	264 (35.5), 279 (33.3), 308 (29.1), 333 (19.3), 393 (9.4), 462 (0.8)	530, 559*, 605	0.62 (0.10)	1.4 (0.23)	4.4	2.7	1.6	508*, 540	17.81
IrL^{10}_2	269 (33.7), 305 (34.6), 317 (34.9), 346 (21.3), 374 (14.8), 390 (12.5), 415 (7.4), 470 (1.0)	555	0.36 (0.03)	4.23 (0.64)	0.9	1.5	1.0	511*, 553, 602, 658	6.46

[a] $Ir(ppy)_3$ in CH_2Cl_2 was used as reference, [b] in deaerated solution unless otherwise mentioned, [c] recorded in butyronitrile, [d] with $[O_2]$ = 2.2 mM in dichloromethane. * denotes the most intense band.

Table 2: photophysical and electrochemical properties in CH_3CN at room temperature.

Complex	absorption λ [nm] (ε × 10^3 [M^{-1} cm^{-1}])	Photoluminescence (278 K)[a,b] in CH_3CN						Electrochemical properties[d]	
		λ [nm]	Φ (air)	τ [µs] (air)	k_r x 10^5 [s^{-1}]	Σk_{nr} x 10^5 [s^{-1}]	$k_Q[O_2]^c$ 10^9 [$M.s^{-1}$]	E^{red} (V)	E^{ox} (V)
IrL^1_2	283 (15.9), 295(17.2), 304 (17.6), 339 (6.8),380 (4.5), 406 (2.7), 479 (0.8)	584	0.20 (0.01)	0.76 (0.07)	2.7	10.5	2.4	-1.87	0.89
IrL^2_2	276 (36.9), 308(35.6), 343 (19.8), 389(12.9), 414 (8,2), 478 (1,2)	577	0.18 (0.02)	0.88 (0.09)	2.0	9.3	1.2	-1.80	0.99
IrL^3_2	271 (26;5), 296(22.7), 305 (25.5), 341 (8.2),385 (5.9), 411 (3.2), 468 (0.3)	589	0.27 (0.02)	0.91 (0.09)	3.0	8.0	1.3	-1.82	0.99
IrL^4_2	286 (26.4), 308(30.1), 316 (32.0), 335 (22.8), 374 (12.2), 405 (6.6), 471 (0.7)	600	0.16 (0.02)	0.64 (0.09)	2.5	13.1	1.1	-1.84	0.86
IrL^5_2	286 (35.1), 298 (40.0), 308 (37.5), 345 (15.5), 382 (10.6), 417 (4.8),	538	0.11 (0.03)	1.24 (0.11)	0.9	7.2	0.2	-1.81	1.14
IrL^6_2	293 (41.4), 305(45.4), 329 (27.4), 361 (17.7), 385 (12.6), 460 (1.4)	589	0.09 (0.01)	0.43 (0.07)	2.2	21.2	1.9	-1.87	0.87
IrL^7_2	270 (30.9), 296(30.3), 307 (30.0), 346 (10.8),384 (7.1), 418 (3.5)	495*, 530, 615	0.50 (0.03)	2.61 (0.16)	1.9	1.9	0.8	-1.75	1.23
IrL^8_2	268 (42.4), 305(35.2), 330 (27.6), 386 (14.8),460 (1.1)	603	0.04 (0.01)	0.26 (0.05)	1.3	36.7	1.3	-1,86	0.76
IrL^9_2	262 (42.8), 278(39.5), 306 (35.3), 330 (22.6),359 (15.4), 388 (10.7), 446 (1.0)	575	0.31(0.03)	1.1 (0.10)	2.9	6.4	1.6	-1.80	1.06
IrL^{10}_2	268 (34.0), 305 (35.8), 316 (35.8), 342 (21.7), 371 (15.0), 389 (12.2), 412 (7.3), 463 (0.9)	528, 562*, 615	0.19(0.01)	4.63 (0.16)	0.4	1.8	1.0	-1.81	0.98

a $Ir(ppy)_3$ in CH_2Cl_2 was used as reference, b in deaerated solution unless otherwise mentioned, c with $[O_2]$ = 9.1 mM in CH_3CN and d Potentials obtained by cyclic voltammetry using Bu_4NPF_6 (0.1 M) as the supporting electrolyte in CH_3CN. Potentials are given relative to the Ag+/Ag couple (Reference electrode ANE2, $AgNO_3$ = 10-2 M) measured under the same conditions. * denotes the most intense band.

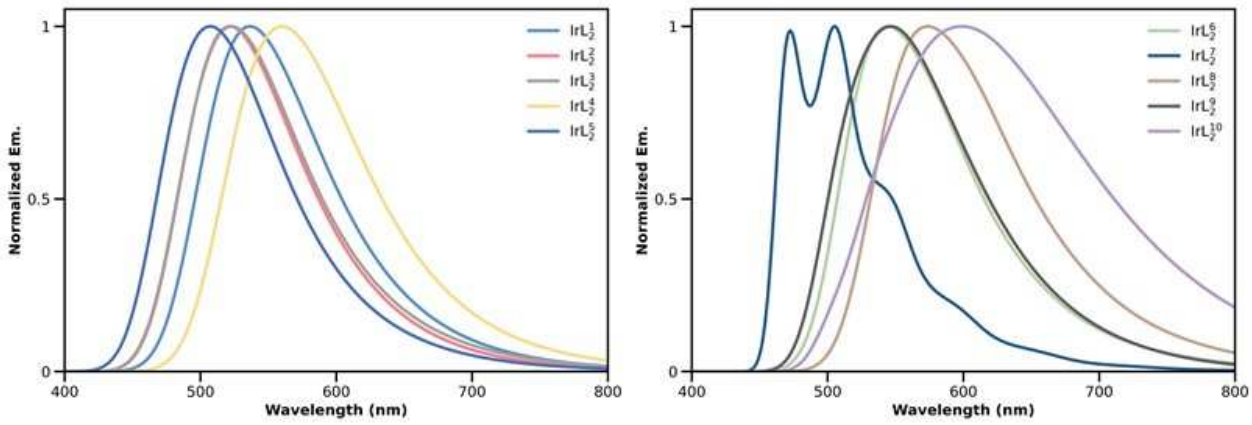

Figure 9: Simulation of emission spectra for Ir complexes.

We now focus the discussion on the electronic transition occurring at the ground state (absorption). The computed transitions (λ_{calc}) and their related oscillator strengths (f) and contributions are reported in Table 1 for f >0.01 and λ_{calc} > 330 nm. The simulated TD-DFT spectra are summarized in **Erreur ! Source du renvoi introuvable.**. In most of the compounds, the computed λ_{calc} fit nicely the experimental absorption data where all spectra present a rather similar shape (**Erreur ! Source du renvoi introuvable.** and Figure S12). For $\mathbf{IrL^1_2}$, the computed weak transition at 429 nm (f = 0.0585) is related to HOMO-1→LUMO (97 %) and may be associated to the experimental one found at 407 nm. This transition is assigned to a mix M/LLCT, due to the participation of the orbitals from the cyclometallating ligands and the Ir(III) site within the HOMO-1 orbital. The second band measured at 383 nm is assigned to the computed one at 388 nm (f = 0.2183), ascribed to the HOMO→LUMO+1 (97 %) transition which corresponds to a MLCT.

Since the ground state properties are well described by the computations, we started to simulate the excited state structures and their related luminescence properties. To do so, we relaxed the structures of the triplets (excited state) using the unrestricted method.[89] The comparison for the first sphere of coordinence for Ir(III) centers between the optimized singlet and triplet states is detailed in SI. Briefly, the Ir-C, Ir-N_{C^N} and Ir-N_{bpy} bonds tends to be slightly reduced within the triplet state to ~2.00 Å, ~2.04 Å and ~2.14 Å, respectively. The good reproduction of the ground and excited states allows us to include vibrational contributions to the electronic transitions and simulate the luminescence spectrum (Figure 9 and Figure S12).

For experimental and theoretical photoluminescence spectra, the CIE coordinates were determined and positioned within the chromaticity diagram represented in Figure 10. Once more, one may observe a similar trend with the experimental data which confirms our aforementioned conclusions. Briefly, we reproduce the hypsochromic shift of the $\mathbf{IrL^2_2}$ (520 nm) emission maximum and bathochromic shift of $\mathbf{IrL^4_2}$ (560 nm) with respect to $\mathbf{IrL^1_2}$ (535 nm). Also, when a -CF_3 ($\mathbf{IrL^5_2}$) or -OH ($\mathbf{IrL^6_2}$) group is present in *para* position of the phenyl group in the cyclometallating ligand, we nicely retrieve a respective hypsochromic (500 nm) and bathochromic shift (550 nm).

Table 3: First vertical spin-allowed transitions of the $\mathbf{IrL^1_2}$ complex with oscillator strength f (>0.01) and λ_{calc} > 330 nm.

λ_{calc}	f	Transition	Assignment
429	0.0585	HOMO-3→LUMO 2%	MLCT + LLCT
		HOMO-1→LUMO 97%	
388	0.2183	HOMO→LUMO+1 97%	MLCT
374	0.0114	HOMO-3→LUMO 5%	MLCT + LLCT
		HOMO→LUMO+2 92%	
368	0.0608	HOMO-3→LUMO 91%	MLCT + LLCT
		HOMO-1→LUMO 2%	+LC
		HOMO→LUMO+2 5%	
345	0.0874	HOMO-3→LUMO+1 2%	MLCT + LLCT
		HOMO-1→LUMO+1 92%	
339	0.1010	HOMO-2→LUMO+1 51%	MLCT + LLCT
		HOMO-1→LUMO+2 44%	
334	0.1714	HOMO-2→LUMO+1 45%	MLCT + LLCT
		HOMO-1→LUMO+2 50%	
331	0.0368	HOMO-5→LUMO 2%	MLCT + LC
		HOMO-2→LUMO+2 6%	
		HOMO→LUMO+4 89%	

The location of the -CF_3 group on the benzimidazole ring ($\mathbf{IrL^3_2}$) induces a smaller hypsochromic shift (518 nm) compared to its position in *para* on the phenyl fragment ($\mathbf{IrL^5_2}$). Fixing a -CF_3 group on the benzimidazole ring, our simulations evidenced that the concomitant presence of -CF_3 ($\mathbf{IrL^7_2}$) or -OH ($\mathbf{IrL^9_2}$) group in *para* position within the phenyl fragment induces respectively hypsochromic (486 nm) and bathochromic shift (527 nm) compared to the $\mathbf{IrL^3_2}$ species. In the situation where -OH is located within the benzimidazole ring, a similar trend is observed when comparing the $\mathbf{IrL^4_2}$ complex to $\mathbf{IrL^8_2}$ and $\mathbf{IrL^{10}_2}$ which show a bathochromic shift of 581 nm and 526 nm, respectively.

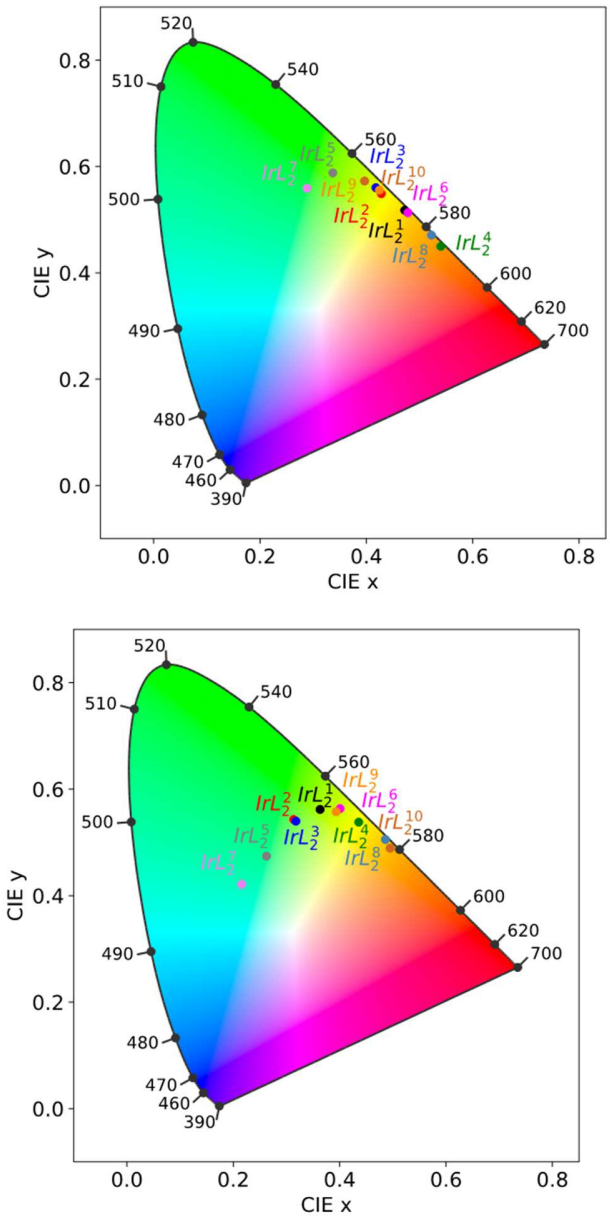

Figure 10: Observed (top) and simulated (bottom) chromaticity CIE(x,y) diagrams.

Conclusions

A series of ten cationic iridium(III) complexes featuring cyclometallating 2-phenylbenzimidazole ligand and 4,4'-dimethyl-2,2'-bipyridine ancillary ligand were developed and fully characterized by the mean of NMR spectroscopy (^{1}H, ^{13}C, ^{19}F and ^{31}P), high resolution mass spectroscopy, UV-Vis and luminescence (steady state and time resolved) spectroscopies, elemental analysis and, finally, first-principles calculations. Single crystal X-ray diffraction obtained from complex **IrL$^{2}_{2}$** displays somewhat rare example of halogen bonding in cyclometallating iridium complexes. We demonstrate that the luminescence and electrochemical properties can be tuned through an original investigation of the influence of the substituent over the benzimidazole moiety, with substituents such as chlorine atoms, -CF_3 and -OMe groups, allowing the emission displayed by the complexes to span from the green to the orange regions of the visible spectrum. In addition, the agonist and antagonist influence of the substituents introduced on both sides of the cyclometallating ligand (i.e. benzimidazole and phenyl moieties) shows synergetic effect, particularly in the case of complex **IrL$^{7}_{2}$**. Complexes **IrL$^{5}_{2}$** and **IrL$^{8}_{2}$** demonstrate properties of switching of the nature of the emitting excited (^{3}M/LLCT* to ^{3}LC*) state by increasing the solvent polarity. Finally, TD-DFT calculations and experimental results allow to attribute the emission to emanate mainly from the radiative deactivation of a mixed excited state ^{3}M/LL'CT* and ^{3}LC* which proportions are dependent on the nature of the substituents and the solvent polarity.

EXPERIMENTAL SECTION

Synthesis

Commercially available reagents were purchased from Sigma-Aldrich, Alfa Aesar, Acros Organics, TCI Chemical, Merck, Strem or Fluorochem and used as received unless otherwise specified. Solvents were obtained from same commercial sources and used without further purification. For moisture sensitive reactions, glassware was oven-dried prior to use. ^{1}H NMR spectra were recorded on a Brucker advance III 400 MHz spectrometer equipped with a BBO probe and on a Brucker advance III 500 MHz spectrometer equipped with a CryoProbe Prodigy in deuterated solvent ($CDCl_3$, DMSO-d^6 or CD_2Cl_2) and data are reported as follows: chemical shift in ppm from tetramethylsilane with the solvent as an internal indicator ($CDCl_3$ 7.26 ppm, dmso-d^6 2.50 ppm, CD_2Cl_2 5.32 ppm), multiplicity (s = singlet, d = doublet, t = triplet, q = quartet, p = pentet, m = multiplet or overlap of non-equivalent resonances), integration. ^{13}C{^{1}H} NMR spectra were recorded either at 101 MHz or at 126 MHz in suitable deuterated solvent and data are reported as follows: chemical shift in ppm from tetramethylsilane with the solvent as an internal indicator ($CDCl_3$ 77.16 ppm, DMSO-d^6 39.52 ppm, CD_2Cl_2 53.84 ppm). ^{19}F NMR spectra were recorded at 376 MHz and at 470 MHz spectrin the suitable deuterated solvent.

Crystal Structures Determinations and Refinements.

Single crystals of compounds **IrL$^{2}_{2}$**, **IrL$^{7}_{2}$** and **IrL$^{10}_{2}$**, were picked up from the mother liquor,

coated with a parafin mixture, collected with nylon loops and mounted on goniometer heads. Measurements were made at 200 K on a Enraf-Nonius 4 circles kappa goniometer equipped with an Incoatec high brilliance microsource with Montel optics monochromated Mo-Kα radiation (λ = 0.71073 Å). The detector was a Bruker APEXII and an Oxford Cryosystem cryostream cooler was used. The crystal data and details of the data collections are given in **Table 1**. The data were integrated and corrected for Lorentz and polarization effects using Eval14,[96] corrected for absorption using SADABS[i] and finaly merged using Xprep[ii]. Crystallographic structures were solved using direct methods implemented by Superflip.[97] Refinement was performed using ShelxL-2013[98] run under Olex2[99]. C, N, O, and Br atoms were refined anisotropically by the full matrix least-squares method on F^2. H atoms were set geometrically.

Supplementary data is available on request from the CCDC, 12 Union Road, Cambridge CB2 1EZ, UK, quoting the deposition number CCDC-2091730, -2091731 and -2091732 for *X*, *Y*, and *Z* respectively. These data can be obtained free of charge at www.ccdc.cam.ac.uk/conts/retrieving.html or fax: +44-1223/336-033; E-mail: deposit@ccdc.cam.ac.uk].

1) Electrochemistry

All electrochemical measurements were performed in a standard three-compartment electrochemical cell under an argon atmosphere. Silver/silver nitrate (ANE2) in CH_3CN ($Ag/AgNO_3$ 10 mM/CH_3CN) and a platinum coil were used as reference and counter electrodes, respectively. Modified carbon electrodes were used as working electrodes. Cyclic voltammograms were recorded with CHI 600 or 630 potentiostats (CH Instruments), allowing on-line ohmic drop compensation.

2) Absorption and emission spectroscopies

Absorption spectra were recorded on a Cary 300 UV−visible spectrophotometer (Varian) and emission spectra (in solution and at 77 K) were recorded on a Fluoromax 4® (Horiba) or on a FLS-1000® (Edinburgh Instruments) equipped with automatic filters to remove the harmonic bands. Quartz cuvette with 1 cm optical path were used. Lifetimes were measures using LP900 spectrometer with a Flashlamp pumped Q-switched Nd:Yag laser operating 355 nm and with photomulitplie (PMT) detector, or with a picosecond laser diode operating at 410 nm and using a time-correlated single photon counting detection (TCSPC, PicoHarp 300).

3) Computational details

Density Functional Theory (DFT) simulations have been performed using the Gaussian16 package.[77] Based on previous theoretical investigations conducted by some of us,[78–81] we considered the B3PW91 functional[82–84] in addition to the LanL2Dz basis set, which includes a pseudopotential to describe core electrons for large atoms together with polarization functions on C (d; 0.587), N (d; 0.736), O (d; 0.961), F (d; 1.577) Cl (d; 0.75) and Ir (f; 0.938).[85–89] The Polarizable Continuum Model (PCM)[90,91] was used to take into account solvent effects (CH_2Cl_2). For computational savings, the -OMe and -NiPr fragments were replaced by -OH and -NH groups. Geometry relaxations of the singlet (ground state) and triplet (excited state) states were per-formed and carefully checked by the calculation of the vibrational frequencies. The general Adiabatic Hessian approach (AH)[92] was considered for estimating vibrational contributions into the computation of emission spectra. Post-treatments were done using the Gaussview and VMS packages.[93–95] Horseshoe plots were realized using an in house Python code.

Synthetic procedures of the proligands (HL)

1) Synthesis of the nitrobenzenamine derivatives

a) General procedure

N-isopropyl-o-nitro-anilines were prepared following the procedure reported by Bünzli *et al*[54] with slight modifications. In a high-pressure flask, under argon atmosphere an excess (2.1 eq) of isopropyl amine (used as base and reagent) were added to a solution of the nitrohaloarenes (1 eq) in DMSO. The solutions were heated at 60 °C overnight and let cool to RT, extracted with diethylether and washed with water to remove DMSO. Purified by flash chromatography (SiO_2) in mixture CH_2Cl_2/C_5H_{12}.

b) Detailed procedures

N-(1-methylethyl)-2-nitrobenzenamine 1: 1-Fluoro-2-nitrobenzene (1.00 g 7.1 mmol), isopropylamine (0.88 g 14.9 mmol), and DMSO (3 mL). SiO_2 (CH_2Cl_2/C_5H_{12} 7:3). Orange liquid (1.00 g 79%) ^{1}H NMR (400 MHz, $CDCl_3$) δ 8.17 (dd, *J* = 8.6, 1.4 Hz, 1H), 8.01 (s, *J* = 44.6 Hz, 1H), 7.41 (ddd, *J* = 8.6, 7.0, 1.5 Hz, 1H), 6.86 (d, *J* = 8.7 Hz, 1H), 6.60 (t, *J* = 7.8 Hz, 1H), 3.83 (hept, *J* = 6.2 Hz, 1H), 1.33 (d, *J* = 6.3 Hz, 6H). ^{13}C NMR (101 MHz, $CDCl_3$) δ 144.9, 136.2, 131.9, 127.2, 115.0, 114.3, 44.0, 22.8. MS (ESI) found *m/z* 180.95 calcd *m/z* 181.10 for $C_9H_{13}N_2O_2$ $[M+H]^+$. Elemental analysis calcd for $C_9H_{12}N_2O_2$ calcd C, 59.99; H, 6.71; N, 15.55 found. C,60.27; H;6.83 N, 15.61.

4,5-dichloro-N-(1-methylethyl)-2-nitrobenzenamine 2: 1,2-Dichloro-4-fluoro-5-nitrobenzene (1.00 g 4.8 mmol), isopropylamine (0.59 g 10.9 mmol) and DMSO (3 mL). Recrystalized from CH_2Cl_2. Orange crystals (1.16 g 97%) ^{1}H NMR (400 MHz, $CDCl_3$) δ 8.28 (s, 1H), 7.91 (s, 1H), 6.97 (s, 1H), 3.77 (dh, *J* = 12.8, 6.5 Hz, 1H), 1.34 (d, *J* = 6.4 Hz, 6H). ^{13}C NMR (101 MHz, $CDCl_3$) δ 143.5, 141.3, 130.5, 128.1, 118.4, 115.4, 44.6, 22.7. MS (ESI) found *m/z* 248.93 calcd *m/z* 249.02 for $C_9H_{10}Cl_2N_2O_2$ $[M+H]^+$. Elemental analysis calcd for $C_9H_{10}Cl_2N_2O_2$ calcd C, 43.40; H, 4.05; N, 11.25 found. C, 43.47; H,4.48; N, 11.56.

N-(1-methylethyl)-2-nitro-(4-trifluoromethyl)benzenamine 3: 4-Bromo-3-nitrobenzotrifluoride (1.00 g 3.7 mmol), isopropylamine (0.44 g 7.4 mmol) and DMSO (3 mL). Recrystalized from CH_2Cl_2. Yellow crystals (0.87 g 95%) ^{1}H NMR (400 MHz, $CDCl_3$) δ 8.47 (d, *J* = 1.1 Hz, 1H), 8.22 (s, 1H), 7.60 (dd, *J* = 9.1, 2.1 Hz, 1H), 6.95 (d, *J* = 9.1 Hz, 1H), 3.88 (dh, *J* = 12.8, 6.4 Hz, 1H), 1.36 (d, *J* = 6.4 Hz, 6H). ^{13}C NMR (101 MHz, $CDCl_3$) δ 146.2, 132.2, 132.2, 132.1, 132.1, 130.9, 127.8, 125.4, 125.3, 125.3, 125.3, 125.1, 122.5, 117.6, 117.3, 116.9, 116.6, 114.9, 44.5, 22.7. ^{19}F NMR (376 MHz, $CDCl_3$) δ -61.9. MS (ESI) found *m/z* 248.98 calcd *m/z* 249.09 for $C_{10}H_{12}F_3N_2O_2$ $[M+H]^+$. Elemental analysis calcd for $C_{10}H_{11}F_3N_2O_2$ calcd C, 48.39; H, 4.47; N, 11.29 found. C, 47.98; H, 4.72; N, 11.08

5-methoxy-N-(1-methylethyl)-2-nitrobenzenamine 4:2-Fluoro-4-methoxy-1-nitrobenzene (1.00 g 5.8 mmol), isopropylamine (0.72 g 12.2 mmol) and DMSO (3 mL). SiO2 (CH_2Cl_2/C_5H_{12} 9:1). Orange liquid (1.17 g 95%) ^{1}H NMR (400 MHz, $CDCl_3$) δ 8.24 (s, 1H), 8.10 (d, *J* = 9.5 Hz, 1H), 6.18 (dd, *J* = 9.5, 2.2 Hz, 1H), 6.14 (d, *J* = 2.2 Hz, 1H), 3.84 (s, 3H), 3.77 (dh, *J* = 12.2, 6.2, 6.2 Hz, 1H), 1.31 (d, *J* = 6.3 Hz, 6H). ^{13}C NMR (101 MHz, $CDCl_3$) δ 166.0, 147.0, 129.4, 126.4, 104.3, 95.6, 55.7, 44.1, 22.6. MS (ESI) found *m/z* 210.97 calcd *m/z* 211.11 for $C_{10}H_{15}N_2O_3$ $[M+H]^+$. Elemental analysis calcd for $C_{10}H_{14}N_2O_3$ calcd C, 57.13; H, 6.71; N, 13.33 found. C, 57.81; H, 6.62; N, 13.2

2) Synthesis of the 2-phenylbenzimidazole derivatives

a) General procedure for the 2-phenylbenzimidazole derivatives

Selected N-isopropyl-o-nitro-anilines (1 eq.) and benzaldehydes (1 eq.) were dissolved in a mixture of 2-ethoxyethanol/water 4:1 (5.4 mL/mmol of nitro-aniline) and heated until dissolution. $Na_2S_2O_4$ (3 eq.) was added to the mixture and refluxed overnight.[100] The reaction mixture was cooled to r.t. and the product extracted with dichloromethane and purified over SiO_2.

b) Detailed procedures

HL^1: N-(1-methylethyl)-2-nitrobenzenamine[101] (0.50 g 2.8 mmol), benzaldehyde (0.294 g 2.8 mmol), $Na_2S_2O_4$ (1.705 g 8.3 mmol) and 2-ethoxyethanol-water 4:1 (15 mL). SiO2 (cyclohexane/ethyl acetate/Et_3N; 64:35:1). White powder (0.37 g 57%). ^{1}H NMR (400 MHz, $CDCl_3$) δ 7.87 – 7.81 (m, 1H), 7.68 – 7.60 (m, 3H), 7.54 – 7.47 (m, 3H), 7.33 – 7.26 (m, 2H), 4.83 (hept, *J* = 7.0 Hz, 1H), 1.66 (d, *J* = 7.0 Hz, 6H). ^{13}C NMR (101 MHz, $CDCl_3$) δ 153.6, 153.6, 143.6, 143.6, 133.6, 131.0, 130.9, 129.9, 129.6, 128.8, 122.5, 122.3, 122.3, 120.4, 112.4, 49.0, 31.0, 21.6. HR-MS (ESI) found *m/z* 237.13844 calcd *m/z* 237.13863 for $C_{16}H_{16}N_2$ $[M+H]^+$. Elemental analysis calcd for $C_{16}H_{16}N_2$ calcd. C, 80.31; H, 6.65; N, 11.53 found. Corresponding with the previous reports of the compound[102]

HL^2: 4,5-dichloro-N-(1-methylethyl)-2-nitrobenzenamine[101] (0.53 g 2.1 mmol), benzaldehyde (0.228 g 2.1 mmol), $Na_2S_2O_4$ (1.320 g 6.4 mmol)

and 2-ethoxyethanol-water 4:1 (15 mL). SiO_2 (CH_2Cl_2/C_5H_{12}/Et_3N; 89:10:1). Low temperature crystallisation in ethyl acetate/cyclohexane. White crystals (0.43 g 65%) ^{1}H NMR (400 MHz, $CDCl_3$) δ 7.89 (s, 1H), 7.71 (s, 1H), 7.65 – 7.59 (m, 2H), 7.54 (q, *J* = 3.5 Hz, 3H), 4.79 (hept, *J* = 6.8 Hz, 1H), 1.62 (d, *J* = 7.0 Hz, 6H). ^{13}C NMR (101 MHz, $CDCl_3$) δ 155.7, 143.3, 132.8, 130.3, 130.2, 129.5, 129.0, 126.3, 126.2, 121.4, 113.5, 49.2, 31.0, 21.5. HRMS (ESI) found *m/z* 305.06038 calcd *m/z* 305.06068 for $C_{16}H_{15}Cl_2N_2$ $[M+H]^+$ Elemental analysis calcd (%) for $C_{16}H_{14}Cl_2N_2$, C, 62.96; H, 4.63; N, 9.18 found C, 62.76; H, 4.86; N, 9.12

HL^3: N-(1-methylethyl)-2-nitro-(4-trifluoromethyl)benzenamine (0.58 g 2.3 mmol), benzaldehyde (0.249 g 2.3 mmol), $Na_2S_2O_4$ (1.443 g 7.0 mmol) and 2-ethoxyethanol-water 4:1 (15 mL). SiO_2 (CH_2Cl_2/C_5H_{12}/Et_3N; 89:1:1). White powder (0.62 g 87%). ^{1}H NMR (400 MHz, $CDCl_3$) δ 8.10 (s, 1H), 7.71 (d, *J* = 8.6 Hz, 1H), 7.68 – 7.60 (m, 2H), 7.57 – 7.48 (m, 4H), 4.85 (hept, *J* = 7.0 Hz, 1H), 1.66 (d, *J* = 7.0 Hz, 6H). ^{13}C NMR (101 MHz, $CDCl_3$) δ 155.7, 143.4, 135.7, 130.5, 130.4, 130.4, 130.3, 130.2, 130.0, 129.8, 129.7, 129.7, 129.5, 129.4, 129.3, 129.2, 129.2, 129.1, 129.1, 129.0, 126.3, 124.5, 119.2, 119.2, 118.1, 118.0, 118.0, 112.7, 112.7, 49.3, 49.2, 21.6. ^{19}F NMR (376 MHz, $CDCl_3$) δ -60.8. HRMS (ESI) found *m/z* 305.12567 calcd *m/z* 305.12601 for $C_{17}H_{16}F_3N_2$ $[M+H]^+$ Elemental analysis calcd (%) for $C_{17}H_{15}F_3N_2$ calcd C, 67.09; H, 4.98; N, 9.21 found C, 66.92; H, 4.91; N, 8.99.

HL^4: 5-methoxy-N-(1-methylethyl)-2-nitrobenzenamine (0.24 g 1.1 mmol), benzaldehyde (0.120 g 1.1 mmol), $Na_2S_2O_4$ (0.693 g 3.4 mmol) and 2-ethoxyethanol-water 3:1 (10 mL). SiO_2 cyclohexane/ethyl acetate/Et_3N (59:40:1). White powder (0.21 g 69%). ^{1}H NMR (400 MHz, $CDCl_3$) δ 7.71 (d, *J* = 8.8 Hz, 1H), 7.65 – 7.59 (m, *J* = 6.5, 3.3 Hz, 2H), 7.53 – 7.45 (m, 2H), 7.08 (d, *J* = 2.3 Hz, 1H), 6.93 (dd, *J* = 8.8, 2.3 Hz, 1H), 4.78 (hept, *J* = 6.9 Hz, 1H), 3.90 (s, 3H), 1.62 (d, *J* = 7.0 Hz, 6H). ^{13}C NMR (101 MHz, $CDCl_3$) δ 156.0, 153.2, 138.6, 134.2, 131.3, 129.5, 129.5, 128.7, 120.7, 110.6, 96.8, 56.1, 48.7, 21.3. HRMS (ESI) found *m/z* 267.14910 calcd *m/z* 267.14919 for $C_{17}H_{19}N_2O$ $[M+H]^+$. Elemental analysis calcd (%) for $C_{17}H_{18}N_2O$, C, 76.66; H, 6.81; N, 10.52 found C, 76.31; H, 6.71; N, 10.59.

HL^5: N-(1-methylethyl)-2-nitrobenzenamine (0.44 g 2.5 mmol), 4-(trifluoromethyl)benzaldehyde (0.427 g 2.5 mmol), $Na_2S_2O_4$ (1.507 g 7.4 mmol) and 2-ethoxyethanol-water 4:1 (15 mL). SiO_2 (CH_2Cl_2/C_5H_{12}/Et_3N; 89:10:1). Low temperature crystallisation in ethyl acetate/cyclohexane. White powder (0.44 g 59%)^{1}H NMR (500 MHz, $CDCl_3$) δ 7.86 – 7.82 (m, 1H), 7.78 (s, 4H), 7.67 – 7.63 (m, 1H), 7.36 – 7.28 (m, 2H), 4.77 (hept, *J* = 6.9 Hz, 1H), 1.67 (d, *J* = 7.0 Hz, 6H). ^{13}C NMR (126 MHz, $CDCl_3$) δ 152.0, 143.9, 134.8, 134.8, 133.7, 132.1, 131.9, 131.6, 131.4, 130.0, 127.2, 125.8, 125.8, 125.8, 125.7, 125.1, 122.9, 122.5, 120.7, 120.7, 112.6, 49.2, 21.6. ^{19}F NMR (470 MHz, $CDCl_3$) δ -62.8 HRMS (ESI) found *m/z* 305.12556 calcd *m/z* 305.12601 for $C_{17}H_{15}F_3N_2$ $[M+H]^+$. Elemental analysis calcd (%) for $C_{17}H_{15}F_3N_2$, C, 67.10; H, 4.97; N, 9.21 found C, 66.78; H, 5.13; N, 9.13.

HL^6: N-(1-methylethyl)-2-nitrobenzenamine (0.57 g 3.1 mmol), 4-methoxybenzaldehyde (0.428 g 3.1 mmol), $Na_2S_2O_4$ (1.930 g 9.4 mmol) and 2-ethoxyethanol-water 4:1 (15 mL). SiO_2 (cyclohexane/ethyl acetate/Et_3N; 64:35:1). White powder (0.32 g 38%). ^{1}H NMR (400 MHz, $CDCl_3$) δ 7.85 – 7.76 (m, 1H), 7.65 – 7.54 (m, 3H), 7.30 – 7.22 (m, 2H), 7.08 – 6.98 (m, 2H), 4.84 (hept, *J* = 7.0 Hz, 1H), 3.88 (s, 3H), 1.65 (d, *J* = 7.0 Hz, 6H). ^{13}C NMR (101 MHz, $CDCl_3$) δ 160.8, 153.7, 143.9, 133.7, 131.0, 123.4, 122.1, 122.0, 120.2, 114.2, 112.3, 55.5, 48.8, 21.5. HRMS (ESI) found *m/z* 267.14899 calcd *m/z* 267.14919 for $C_{17}H_{19}N_2O$ $[M+H]^+$. Elemental analysis calcd for $C_{17}H_{18}N_2O$ calcd C, 76.66; H, 6.81; N, 10.52 found C, 77.23; H, 6.93; N, 10.55. Corresponding with the previous reports of the compound[103]

HL^7: N-(1-methylethyl)-2-nitro-(4-trifluoromethyl)benzenamine (0.30 g 1.2 mmol), 4-(trifluoromethyl)benzaldehyde (0.209 g 1.2 mmol), $Na_2S_2O_4$ (0.738 g 3.6 mmol) and 2-ethoxyethanol-water 4:1 (10 mL). SiO_2 (CH_2Cl_2/C_5H_{12}/Et_3N; 89:10:1). Low temperature crystallisation in ethyl acetate/cyclohexane as pale

greenish crystals (0.22 g 50%) ^{1}H NMR (400 MHz, $CDCl_3$) δ 8.17 (s, 1H), 7.89 – 7.79 (m, 4H), 7.76 (d, *J* = 8.8 Hz, 1H), 7.59 (d, *J* = 8.8 Hz, 1H), 4.83 (hept, *J* = 6.8 Hz, 1H), 1.71 (d, *J* = 6.8 Hz, 6H). ^{13}C NMR (101 MHz, $CDCl_3$) δ 153.4, 141.7, 135.1, 132.9, 132.8, 132.6, 130.2, 126.2, 126.2, 126.1, 126.1, 126.0, 125.1, 123.3, 122.4, 120.3, 120.3, 120.2, 117.9, 117.9, 117.8, 113.2, 49.9, 21.7. ^{19}F NMR (376 MHz, $CDCl_3$) δ -61.0, -63.0. HRMS (ESI) found *m/z* 373.11299 calcd 373.11339 for $C_{18}H_{15}F_6N_2$ $[M+H]^+$. Elemental analysis calcd for $C_{18}H_{14}F_6N_2$ calcd C, 58.07; H, 3.79; N, 7.52 found C, 58.65; H, 3.69; N, 7.55.

HL^8: 5-methoxy-N-(1-methylethyl)-2-nitrobenzenamine (0.50 g 2.4 mmol), 4-methoxybenzaldehyde (0.325 g 2.4 mmol), $Na_2S_2O_4$ (1.248 g 7.2 mmol) and 2-ethoxyethanol-water 4:1 (15 mL). SiO_2 (cyclohexane/ethyl acetate/Et_3N; 59:40:1). White powder (0.32 g 46%). ^{1}H NMR (400 MHz, $CDCl_3$) δ 7.68 (d, *J* = 8.8 Hz, 1H), 7.60 – 7.52 (m, 2H), 7.07 (d, *J* = 2.3 Hz, 1H), 7.06 – 6.99 (m, 2H), 6.92 (dd, *J* = 8.8, 2.3 Hz, 1H), 4.78 (hept, *J* = 7.0 Hz, 1H), 3.89 (d, *J* = 9.2 Hz, 6H), 1.62 (d, *J* = 7.0 Hz, 6H). ^{13}C NMR (101 MHz, $CDCl_3$) δ 160.7, 155.8, 153.2, 138.6, 134.2, 130.9, 123.6, 120.5, 114.2, 110.4, 96.9, 56.2, 55.5, 48.6, 21.3. HRMS (ESI) *m/z* found 297.15924 calcd *m/z* 297.15975 for $C_{18}H_{21}N_2O_2$ $[M+H]^+$. Elemental analysis calcd for $C_{18}H_{20}N_2O_2$ calcd C, 72.95; H, 6.80; N, 9.45, found C, 72.70; H, 6.69; N, 9.36.

HL^9: N-(1-methylethyl)-2-nitro-(4-trifluoromethyl)benzenamine (0.52 g 2.1 mmol), 4-methoxybenzaldehyde (0.286 g 2.1 mmol), $Na_2S_2O_4$ (1.292 g 6.3 mmol) and 2-ethoxyethanol-water 4:1 (15 mL). SiO_2 (CH_2Cl_2/C_5H_{12}/Et_3N; 89:10:1). Low temperature crystallisation in ethyl acetate/cyclohexane as beige crystals (0.46 g 65%) ^{1}H NMR (400 MHz, $CDCl_3$) δ 8.06 (s, 1H), 7.68 (d, *J* = 8.5 Hz, 1H), 7.57 (d, *J* = 8.5 Hz, 2H), 7.48 (d, *J* = 8.5 Hz, 1H), 7.04 (d, *J* = 8.3 Hz, 2H), 4.85 (hept, *J* = 6.9 Hz, 1H), 3.87 (s, 3H), 1.64 (d, *J* = 6.8 Hz, 6H). ^{13}C NMR (101 MHz, $CDCl_3$) δ 161.1, 155.7, 143.4, 135.7, 130.9, 130.6, 129.0, 126.3, 125.0, 124.6, 124.3, 124.0, 123.6, 122.6, 120.9, 118.9, 118.9, 117.7, 117.7, 114.4, 112.5, 55.5, 49.1, 21.5. ^{19}F NMR (376 MHz, $CDCl_3$) δ -60.8. HRMS (ESI) found *m/z* 335.13603 calcd *m/z* 335.13657 for $C_{18}H_{18}F_3N_2O$ $[M+H]^+$. Elemental analysis calcd for $C_{18}H_{17}F_3N_2O$ calcd C, 64.66; H, 5.13; N, 8.38; found 64.73; H, 5.27; N, 8.51

HL^{10}: 5-methoxy-N-(1-methylethyl)-2-nitrobenzenamine (0.54 g 2.6 mmol), 4-(trifluoromethyl)benzaldehyde (0.447 g 2.6 mmol), $Na_2S_2O_4$ (1.578 g 7.2 mmol) and 2-ethoxyethanol-water 4:1 (15 mL). SiO_2 (CH_2Cl_2/C_5H_{12} 9:1). Low temperature crystallisation in ethyl acetate/cyclohexane as white crystals (0.63 g 73%). ^{1}H NMR (400 MHz, $CDCl_3$) δ 7.81 – 7.74 (m, 4H), 7.72 (d, *J* = 8.8 Hz, 1H), 7.09 (s, 1H), 6.96 (d, *J* = 8.8 Hz, 1H), 4.74 (hept, *J* = 6.8 Hz, 1H), 3.91 (s, 3H), 1.66 (d, *J* = 6.8 Hz, 6H). ^{13}C NMR (101 MHz, $CDCl_3$) δ 156.4, 151.5, 138.6, 134.4, 130.0, 125.8, 125.8, 125.8, 121.0, 111.2, 96.8, 56.2, 49.0, 21.4. ^{19}F NMR (376 MHz, $CDCl_3$) δ -62.8. HRMS (ESI) found *m/z* 335.13624 calcd *m/z* 335.13657 for $C_{18}H_{18}F_3N_2O$ $[M+H]^+$. Elementary analysis calcd for $C_{18}H_{17}F_3N_2O$ calcd C, 64.66; H, 5.13; N, 8.38; found C, 64.50; H, 5.22; N, 8.54

Synthesis of the complexes

a) General procedure

From the compounds **HL^1** – **HL^{10}**, The chloro-bridged Ir(III) dimers $[Ir(L)_2(\mu\text{-}Cl)]_2$ were synthesized following the method of Watts[55], an excess (2.5-3 eq.) of ligand **HL** and $IrCl_3{\cdot}xH_2O$ were refluxed overnight in a mixture of 2-ethoxyethanol/H_2O (3:1). At r.t., water was added and the precipitate were filtered off, washed heavily with water, then with MeOH and Et_2O. After drying, the crude products were used without further purification. The chloro-bridged dimers and 4,4′-dimethyl-2,2′-dipyridyl were dissolved/suspended in a mixture CH_2Cl_2/MeOH 1:1 and refluxed overnight. The mixture was cooled to r.t. and reduced to ¼ of the volume, a saturated solution of KPF_6 (aq.) was added until precipitation and stirred 5-10 min. The precipitated was filtrated and purified over pre-treated SiO_2 with Et_2N with CH_2Cl_2/acetone or CH_2Cl_2/MeOH as eluent.

b) Detailed procedures

IrL^1_2: HL^1 (0.133 g 0.6 mmol), $IrCl_3{\cdot}xH_2O$ (0.08 g 0.2 mmol) and 2-ethoxyethanol/H_2O 3:1 (6 mL), crude. $[Ir(\mathbf{L^1})_2(\mu\text{-}Cl)]_2$ (0.057 g 0.01 mmol), 4,4′-dimethyl-2,2′-dipyridyl (0.015 g 0.01 mmol) and

CH_2Cl_2/MeOH 1:1 (10mL). SiO_2 (CH_2Cl_2/C_3H_6O 9:1) bright orange crystals (48 mg, 60%) were obtained upon slow diffusion of diisopropylether in $C_2H_4Cl_2$. ^{1}H NMR (500 MHz, CD_2Cl_2) δ 8.20 (s, 1H), 7.91 (d, *J* = 5.6 Hz, 1H), 7.84 (d, *J* = 7.9 Hz, 1H), 7.69 (d, *J* = 8.4 Hz, 1H), 7.28 – 7.19 (m, 2H), 7.12 – 7.05 (dt, , *J* = 7.1 Hz 1H), 6.93 (t, *J* = 7.7 Hz, 1H), 6.84 (td, *J* = 7.5, 1.0 Hz, 1H), 6.31 (d, *J* = 6.9 Hz, 1H), 5.81 (d, *J* = 8.3 Hz, 1H), 5.73 (hept, 7.0 Hz, 1H), 2.59 (s, 3H), 1.83 (dd, *J* = 6.9, 3.9 Hz, 6H). ^{13}C NMR (126 MHz, CD_2Cl_2) δ 163.5, 156.9, 153.2, 151.9, 151.2, 140.7, 134.9, 134.2, 134.0, 130.9, 129.1, 126.1, 124.9, 124.3, 123.4, 122.7, 115.1, 114.7, 50.7, 22.0, 21.8. ^{31}P NMR (202 MHz, CD_2Cl_2) δ -133.9, -137.4, -140.9, -140.9, -140.9, -144.4, -144.4, -144.5, -147.9, -147.9, -148.0, -151.4, -155.0. ^{19}F NMR (470 MHz, CD_2Cl_2) δ -72.5, -74.0. HRMS (ESI) found *m/z* 847.30771 calcd *m/z* 847.30974 for $C_{44}H_{42}IrN_6$ $[M\text{-}PF_6]^+$. Elemental Analysis calcd (%) for $C_{44}H_{42}F_6IrN_6P{\cdot}C_2H_4Cl_2$, C, 50.26; H, 4.25; N, 7.70, found C, 51.08; H, 4.27; N, 8.22

IrL$^2_2$: HL^2 (0.114 g 0.06 mmol), $IrCl_3{\cdot}xH_2O$ (0.05 g 0.2 mmol) and 2-ethoxyethanol/H_2O (6 mL), crude. $[Ir(\mathbf{L^2})_2(\mu\text{-}Cl)]_2$ (0.10 g 0.01 mmol), 4,4′-dimethyl-2,2′-dipyridyl (0.022 g 0.01 mmol) and CH_2Cl_2/MeOH 1:1 (10mL). Pale yellow powder (136 mg, 99%) was obtained after precipitation and washed with MeOH and diethylether. ^{1}H NMR (500 MHz, CD_2Cl_2) δ 8.27 (s, 1H), 7.91 (d, *J* = 5.6 Hz, 1H), 7.86 (d, *J* = 7.9 Hz, 1H), 7.80 (s, 1H), 7.34 (d, *J* = 4.9 Hz, 1H), 7.17 – 7.08 (m, 1H), 6.90 (td, *J* = 7.5, 1.0 Hz, 1H), 6.32 (dd, *J* = 7.7, 0.8 Hz, 1H), 5.69 (hept, *J* = 13.6, 6.7 Hz, 1H), 5.61 (s, 1H), 2.64 (s, 3H), 1.81 (dd, *J* = 7.0, 1.6 Hz, 6H). ^{13}C NMR (126 MHz, CD_2Cl_2) δ 165.6, 156.9, 153.2, 152.7, 151.5, 139.9, 134.2, 134.0, 133.2, 131.7, 129.2, 128.6, 127.3, 126.7, 125.3, 123.2, 116.1, 115.7, 51.2, 22.0, 21.8, 21.8. ^{31}P NMR (202 MHz, CD_2Cl_2) δ -133.9, -137.4, -140.9, -144.4, -147.9, -151.4, -155.0. ^{19}F NMR (470 MHz, CD_2Cl_2) δ -72.4, -73.9. HRMS (ESI) found *m/z* 983.15088 calcd *m/z* 983.15155 for $C_{44}H_{38}Cl_4IrN_6$ $[M\text{-}PF_6]^+$. Elemental Analysis calcd (%) for $C_{44}H_{38}Cl_4F_6IrN_6P$, C, 46.77; H, 3.39; N, 7.44; found C, 46.80; H, 3.33; N, 7.65.

IrL$^3_2$: HL^3 (0.246 g 0.08 mmol), $IrCl_3{\cdot}xH_2O$ (0.115 g 0.04 mmol) and 2-ethoxyethanol/H_2O (6 mL), crude. $[Ir(\mathbf{L^3})_2(\mu\text{-}Cl)]_2$ (0.060 g 0.01 mmol), 4,4′-dimethyl-2,2′-dipyridyl (0.013 g 0.01 mmol) and CH_2Cl_2/MeOH 1:1 (10mL). SiO_2 (CH_2Cl_2/C_3H_6O 9/1) and isolated as yellow powder (41 mg, 50%) ^{1}H NMR (500 MHz, CD_2Cl_2) δ 8.21 (s, 1H), 7.97 (d, *J* = 5.6 Hz, 1H), 7.89 (d, *J* = 8.0 Hz, 1H), 7.82 (d, *J* = 8.7 Hz, 1H), 7.48 (d, *J* = 8.7 Hz, 1H), 7.33 (d, *J* = 5.5 Hz, 1H), 7.14 (t, *J* = 7.6 Hz, 1H), 6.90 (t, *J* = 7.5 Hz, 1H), 6.33 (d, *J* = 7.6 Hz, 1H), 5.84 – 5.70 (m, 2H), 2.61 (s, 3H), 1.85 (dd, *J* = 6.8, 5.0 Hz, 6H). ^{13}C NMR (126 MHz, CD_2Cl_2) δ 165.8, 157.0, 153.4, 152.8, 151.7, 140.1, 136.1, 134.2, 134.1, 131.8, 129.2, 127.8, 126.8, 126.5, 126.2, 126.0, 125.6, 125.1, 123.4, 123.2, 121.3, 120.2, 120.2, 115.2, 112.4, 112.4, 112.3, 112.3, 51.3, 22.1, 21.8, 21.7. ^{31}P NMR (202 MHz, CD_2Cl_2) δ -133.9, -137.4, -141.0, -144.5, -148.0, -151.5, -155.0. ^{19}F NMR (470 MHz, CD_2Cl_2) δ -62.0, -72.7, -74.2. HRMS (ESI) found *m/z* 983.28155 calcd *m/z* 983.28453 for $C_{46}H_{40}F_6IrN_6$ $[M\text{-}PF_6]^+$. Elemental Analysis calcd (%) $C_{46}H_{40}F_{12}IrN_6P$ calcd C, 48.97; H, 3.58; N, 7.45, found C, 49.09; H, 3.42; N, 7.62

IrL$^4_2$: HL^4 (0.219 g 0.08 mmol), $IrCl_3{\cdot}xH_2O$ (0.117 g 0.04 mmol) and 2-ethoxyethanol/H_2O (6 mL), crude. $[Ir(\mathbf{L^4})_2(\mu\text{-}Cl)]_2$ (0.085 g 0.01 mmol), 4,4′-dimethyl-2,2′-dipyridyl (0.021 g 0.01 mmol) and CH_2Cl_2/MeOH 1:1 (10mL). SiO_2 (CH_2Cl_2/C_3H_6O/Et_3N 89:10:1) isolated as bright yellow/orange powder (63 mg, 53%) ^{1}H NMR (500 MHz, CD_2Cl_2) δ 8.32 (s, 1H), 7.98 (d, *J* = 5.6 Hz, 1H), 7.80 (d, *J* = 7.8 Hz, 1H), 7.54 (d, *J* = 9.1 Hz, 1H), 7.27 (dd, *J* = 5.6, 0.9 Hz, 1H), 7.12 – 7.03 (m, 1H), 6.90 – 6.78 (m, 2H), 6.35 (dd, *J* = 7.7, 0.9 Hz, 1H), 5.67 (hept, *J* = 13.8, 6.8 Hz, 1H), 5.27 (d, *J* = 2.4 Hz, 1H), 3.23 (s, 3H), 2.56 (s, 3H), 1.80 (dd, *J* = 6.9, 2.8 Hz, 6H). ^{13}C NMR (126 MHz, CD_2Cl_2) δ 163.11, 157.47, 157.18, 152.72, 151.95, 151.41, 141.73, 135.02, 134.24, 130.70, 128.98, 128.19, 125.73, 125.11, 122.74, 115.08, 113.56, 96.93, 55.55, 50.60, 22.19, 21.93, 21.57, 1.32.^{31}P NMR (202 MHz, CD_2Cl_2) δ -133.86, -137.37, -140.88, -144.39, -147.91, -151.42, -154.93. ^{19}F NMR (470 MHz, CD_2Cl_2) δ -72.37, -73.88. HRMS (ESI) found *m/z* 907.32846 calcd *m/z* 907.33089 for $C_{46}H_{46}IrN_6O_2$ $[M+PF_6]^+$. Elemental

Analysis calcd (%) for $C_{46}H_{46}F_6IrN_6O_2P$, C, 52.51; H, 4.41; N, 7.99, found C, 52.75; H, 4.59; N, 8.11.

IrL^5_2: HL^5 (0.235 g 0.8 mmol), $IrCl_3{\cdot}xH_2O$ (0.11 g 0.4 mmol) and 2-ethoxyethanol/H_2O (6 mL), crude. $[Ir(L^1)_2(\mu\text{-}Cl)]_2$ (0.093 g 0.01 mmol), 4,4′-dimethyl-2,2′-dipyridyl (0.021 g 0.01 mmol) and CH_2Cl_2/MeOH 1:1 (10mL). SiO_2 (CH_2Cl_2/C_3H_6O/Et_3N 89:10:1) and isolated as yellow powder (67 mg 54%). ^{1}H NMR (500 MHz, CD_2Cl_2) δ 8.29 (d, *J* = 6.3 Hz, 1H), 7.91 (d, *J* = 8.3 Hz, 1H), 7.83 (d, *J* = 5.6 Hz, 1H), 7.75 (d, *J* = 8.4 Hz, 1H), 7.38 – 7.22 (m, 3H), 7.00 (t, *J* = 7.8 Hz, 1H), 6.36 (s, 1H), 5.84 (d, *J* = 8.3 Hz, 1H), 5.68 (hept, *J* = 6.7 Hz, 1H), 2.62 (s, 1H), 1.85 (dd, *J* = 40.6, 6.9 Hz, 6H) ^{13}C NMR (126 MHz, CD_2Cl_2) δ 162.1, 156.9, 152.9, 152.7, 151.3, 140.4, 138.6, 133.9, 131.9, 131.6, 131.4, 131.1, 129.4, 129.4, 129.4, 127.4, 126.0, 125.3, 125.2, 125.2, 124.4, 123.0, 120.9, 120.0, 119.9, 115.3, 114.9, 51.3, 21.9, 21.8, 21.7. ^{31}P NMR (202 MHz, CD_2Cl_2) δ -133.9, -137.4, -140.9, -144.4, -147.9, -151.4, -155.0. ^{19}F NMR (470 MHz, CD_2Cl_2) δ -63.5, -72.4, -73.9. HRMS (ESI) found *m/z* 983.28156 calcd *m/z* 983.28453 for $C_{46}H_{40}F_6IrN_6$ $[M\text{-}PF_6]^+$. Elemental Analysis calcd (%) $C_{46}H_{40}F_{12}IrN_6P$, C, 48.97; H, 3.58; N, 7.45, found C, 48.88; H, 3.50; N, 7.69

IrL^6_2: HL^6 (0.259 g 1.0 mmol), $IrCl_3{\cdot}xH_2O$ (0.138 g 0.5 mmol) and 2-ethoxyethanol/H_2O (6 mL), crude. $[Ir(\mathbf{L^6})_2(\mu\text{-}Cl)]_2$ (0.085 g 0.01 mmol), 4,4′-dimethyl-2,2′-dipyridyl (0.021 g 0.01 mmol) and CH_2Cl_2/MeOH 1:1 (10mL). SiO_2 (CH_2Cl_2/C_3H_6O/Et_3N 89:10:1) isolated as orange powder (63 mg 53%) ^{1}H NMR (500 MHz, CD_2Cl_2) δ 8.19 (s, 1H), 7.93 (d, *J* = 5.6 Hz, 1H), 7.79 (d, *J* = 8.8 Hz, 1H), 7.64 (d, *J* = 8.3 Hz, 1H), 7.26 (d, *J* = 5.5 Hz, 1H), 7.19 (t, *J* = 7.8 Hz, 1H), 6.91 (t, *J* = 7.8 Hz, 1H), 6.65 (dd, *J* = 8.8, 2.6 Hz, 1H), 5.79 (d, *J* = 8.2 Hz, 1H), 5.76 (d, *J* = 2.6 Hz, 1H), 5.64 (hept, *J* = 6.7 Hz, 1H), 3.39 (s, 3H), 2.59 (s, 3H), 1.81 (dd, *J* = 20.2, 6.9 Hz, 6H). ^{13}C NMR (126 MHz, CD_2Cl_2) δ 163.6, 161.4, 156.9, 155.9, 151.9, 151.3, 140.7, 133.8, 129.1, 127.5, 127.3, 124.8, 124.1, 123.0, 118.7, 114.7, 114.2, 108.7, 55.0, 50.5, 21.9, 21.8, 21.7. ^{31}P NMR (202 MHz, CD_2Cl_2) δ -133.9, -137.4, -140.9, -144.4, -147.9, -151.5, -155.0. ^{19}F NMR (470 MHz, CD_2Cl_2) δ -72.5, -74.1. HRMS (ESI) found *m/z* 907.32826 calcd *m/z* 907.33089 for $C_{46}H_{46}IrN_6O_2$ $[M\text{-}PF_6]^+$. Elemental Analysis calcd (%) for $C_{46}H_{46}F_6IrN_6O_2P$, C, 52.51; H, 4.41; N, 7.99, found C, 52.35; H, 4.39; N, 8.06.

IrL^7_2: HL^7 (0.233 g 0.6 mmol), $IrCl_3{\cdot}xH_2O$ (0.089 g 0.3 mmol) and 2-ethoxyethanol/H_2O (6 mL), crude. $[Ir(\mathbf{L^7})_2(\mu\text{-}Cl)]_2$ (0.084 g 0.01 mmol), 4,4′-dimethyl-2,2′-dipyridyl (0.016 g 0.01 mmol) and CH_2Cl_2/MeOH 1:1 (10mL). SiO_2 (CH_2Cl_2/MeOH 95:5) and isolated as bright yellow powder (95 mg 87%). ^{1}H NMR (500 MHz, CD_2Cl_2) δ 8.32 (s, 1H), 8.00 (d, *J* = 8.2 Hz, 1H), 7.94 – 7.86 (m, 2H), 7.56 (dd, *J* = 8.8, 0.8 Hz, 1H), 7.42 – 7.34 (m, 2H), 6.38 (s, 1H), 5.80 (s, 1H), 5.75 (hept, *J* = 7.0 Hz, 1H), 2.64 (s, 3H), 1.87 (dd, *J* = 30.1, 6.9 Hz, 6H). ^{13}C NMR (126 MHz, CD_2Cl_2) δ 164.4, 156.9, 153.6, 152.9, 151.8, 139.8, 137.8, 137.8, 136.0, 132.4, 132.1, 131.9, 129.5, 129.4, 129.3, 129.3, 129.3, 127.6, 127.5, 127.2, 127.2, 127.0, 126.8, 126.7, 125.5, 125.4, 125.0, 123.2, 122.9, 121.2, 121.2, 121.1, 120.7, 120.4, 120.4, 120.4, 115.8, 112.7, 112.7, 112.6, 112.6, 51.8, 22.0, 21.7, 21.7. ^{31}P NMR (202 MHz, CD_2Cl_2) δ -133.9, -137.4, -140.9, -144.4, -147.9, -151.5, -155.0. ^{19}F NMR (470 MHz, CD_2Cl_2) δ -62.2, -63.6, -72.5, -74.0. HRMS (ESI) found *m/z* 1119.25818 calcd *m/z* 1119.25932 for $C_{48}H_{38}F_{12}IrN_6$ $[M\text{-}PF_6]^+$ Elemental Analysis calcd (%) for $C_{48}H_{38}F_{18}IrN_6P$, C, 45.60; H, 3.04; N, 6.65; found C, 45.59; H, 3.17; N, 6.54.

IrL^8_2: HL^8 (0.135 g 0.5 mmol), $IrCl_3{\cdot}xH_2O$ (0.065 g 0.2 mmol) and 2-ethoxyethanol/H_2O (6 mL), crude. $[Ir(\mathbf{L^8})_2(\mu\text{-}Cl)]_2$ (0.077 g 0.1 mmol), 4,4′-dimethyl-2,2′-dipyridyl (0.017 g 0.1 mmol) and CH_2Cl_2/MeOH 1:1 (10mL). SiO_2 (CH_2Cl_2/MeOH 95:5) Bright orange crystals (71 mg, 67%) were obtained upon slow diffusion of diisopropylether in $C_2H_4Cl_2$. ^{1}H NMR (500 MHz, CD_2Cl_2) δ 8.20 (s, 1H), 7.92 (d, *J* = 5.6 Hz, 1H), 7.74 (d, *J* = 8.8 Hz, 1H), 7.25 (dd, *J* = 5.6, 0.9 Hz, 1H), 7.08 (d, *J* = 2.3 Hz, 1H), 6.63 (dd, *J* = 8.8, 2.7 Hz, 1H), 6.54 (dd, *J* = 9.0, 2.3 Hz, 1H), 5.78 (d, *J* = 2.6 Hz, 1H), 5.65 (d, *J* = 9.0 Hz, 1H), 5.60 (hept, *J* = 6.8 Hz, 1H), 3.80 (s, 1H), 3.43 (s, 1H), 2.59 (s, 1H), 1.79 (dd, *J* = 17.3, 7.0 Hz, 1H). ^{13}C NMR (126 MHz,

CD_2Cl_2) δ 163.0, 161.1, 156.9, 156.5, 155.3, 151.8, 151.3, 135.1, 134.5, 129.0, 127.7, 127.0, 124.8, 118.7, 115.2, 112.4, 108.3, 98.5, 56.5, 55.1, 50.2, 21.8, 21.7, 21.5. ^{31}P NMR (202 MHz, CD_2Cl_2) δ -133.9, -137.4, -140.9, -144.4, -147.9, -151.5, -155.0. ^{19}F NMR (470 MHz, CD_2Cl_2) δ -72.5, -74.0 HRMS (ESI) found *m/z* 965.34932 calcd *m/z* 965.34940 for $C_{48}H_{50}O_4IrN_6$ $[M\text{-}PF_6]^+$ Elemental Analysis calcd (%) for $C_{48}H_{50}F_6IrN_6O_4P$ calcd C, 51.84; H, 4.53; N, 7.56, found C, 51.61; H, 4.46; N, 7.75

IrL^9_2: HL^9 (0.198 g 0.6 mmol), $IrCl_3{\cdot}xH_2O$ (0.084 g 0.3 mmol) and 2-ethoxyethanol/H_2O (6 mL), crude. $[Ir(\mathbf{L^9})_2(\mu\text{-}Cl)]_2$ (0.090 g 0.1 mmol), 4,4′-dimethyl-2,2′-dipyridyl (0.019 g 0.1 mmol) and CH_2Cl_2/MeOH 1:1 (10mL). SiO_2 (CH_2Cl_2/MeOH 95:5) isolated as bright yellow powder (116 mg, 96%). ^{1}H NMR (500 MHz, CD_2Cl_2) δ 8.18 (s, 1H), 8.01 (d, *J* = 5.6 Hz, 1H), 7.84 (d, *J* = 9.0 Hz, 1H), 7.75 (d, *J* = 8.7 Hz, 1H), 7.43 (dd, *J* = 8.9, 1.2 Hz, 1H), 7.34 (dd, *J* = 5.6, 0.9 Hz, 1H), 6.70 (dd, *J* = 8.9, 2.6 Hz, 1H), 5.79 (d, *J* = 2.6 Hz, 1H), 5.74 (s, 1H), 5.67 (hept, *J* = 7.0 Hz, 1H), 3.47 (s, 3H), 2.61 (s, 3H), 1.82 (dd, *J* = 6.9, 3.7 Hz, 6H). ^{13}C NMR (126 MHz, CD_2Cl_2) δ 165.77, 162.00, 156.95, 155.94, 152.68, 151.78, 140.18, 135.99, 133.18, 129.23, 128.29, 126.48, 124.98, 119.87, 119.85, 119.82, 119.07, 114.81, 111.85, 111.82, 111.78, 109.21, 108.72, 55.22, 51.02, 22.02, 21.73, 21.72.^{31}P NMR (202 MHz, CD_2Cl_2) δ -137.46, -140.98, -144.49, -148.00, -151.51. ^{19}F NMR (470 MHz, CD_2Cl_2) δ -61.95, -72.69, -74.20. HRMS (ESI) found *m/z* 1043.30569 calcd *m/z* 1043.30489 for $C_{48}H_{44}F_6O_2IrN_6$ $[M\text{-}PF_6]^+$ Elemental Analysis calcd (%) for $C_{48}H_{44}F_{12}IrN_6O_2P{\cdot}CH_3OH$, C, 48.52; H, 3.74; N, 7.07 found C, 47.87; H, 3.70; N, 7.24

IrL^{10}_2: HL^{10} (0.235 g 0.7 mmol), $IrCl_3{\cdot}xH_2O$ (0.100 g 0.3 mmol) and 2-ethoxyethanol/H_2O (6 mL), crude. $[Ir(\mathbf{L^{10}})_2(\mu\text{-}Cl)]_2$ (0.100 g 0.1 mmol), 4,4′-dimethyl-2,2′-dipyridyl (0.021 g 0.1 mmol) and CH_2Cl_2/MeOH 1:1 (10mL). SiO_2 (CH_2Cl_2/MeOH 95:5) isolated as bright yellow powder (133 mg 77%). ^{1}H NMR (500 MHz, CD_2Cl_2) δ 8.30 (s, 1H), 7.86 (d, *J* = 8.4 Hz, 1H), 7.82 (d, *J* = 5.6 Hz, 1H), 7.32 (dd, *J* = 8.3, 1.3 Hz, 1H), 7.27 (dd, *J* = 5.6, 0.8 Hz, 1H), 7.14 (d, *J* = 2.3 Hz, 1H), 6.63 (dd, *J* = 9.1, 2.4 Hz, 1H), 6.38 (d, *J* = 1.5 Hz, 1H), 5.69 (d, *J* = 9.0 Hz, 1H), 5.63 (hept, *J* = 6.9 Hz, 1H), 3.84 (s, 3H), 2.62 (s, 3H), 1.86 (d, *J* = 7.0 Hz, 3H), 1.79 (d, *J* = 7.0 Hz, 3H). ^{13}C NMR (126 MHz, CD_2Cl_2) δ 161.3, 157.4, 156.8, 152.6, 152.3, 151.3, 139.0, 139.0, 134.8, 134.8, 131.4, 131.2, 131.0, 130.7, 129.3, 129.3, 127.5, 125.4, 125.3, 125.3, 123.1, 119.9, 119.9, 119.9, 119.8, 115.9, 114.1, 98.4, 56.5, 50.9, 21.8, 21.6, 21.5.^{31}P NMR (202 MHz, CD_2Cl_2) δ -133.9, -137.4, -140.9, -144.4, -147.9, -151.4, -154.9. ^{19}F NMR (470 MHz, CD_2Cl_2) δ -63.3, -72.3, -73.8. HRMS (ESI) found *m/z* 1043.30269 calcd *m/z* 1043.30569 for $C_{48}H_{44}F_6IrN_6O_2$ $[M+PF_6]^+$. Elemental Analysis calcd (%) for $C_{48}H_{44}F_{12}IrN_6O_2P$, C, 48.52; H, 3.74; N, 7.07 found C, 48.55; H, 3.59; N, 7.32

AUTHOR INFORMATION

Corresponding Authors

Dr. Pierre-Henri Lanoë and Pr. Frédérique Loiseau Univ. Grenoble Alpes, CNRS, DCM, 38000 Grenoble, France, E-mails: frederique.loiseau@univ-grenoble-alpes.fr, pierre-henri.lanoe@univ-grenoble-alpes.fr

Camille Latouche Université de Nantes, CNRS, Institut des Matériaux Jean Rouxel, IMN, F-44000 Nantes, France, E-mail: camille.latouche@univ-nantes.fr

Author Contributions

The manuscript was written through contributions of all authors. / All authors have given approval to the final version of the manuscript.

Funding Sources

This work benefited from state aid managed by the National Research Agency under the "Investments for the future" and of the "Investissements d'avenir" program bearing the reference ANR-15-IDEX-02. E. Martinez-Vollbert benefits of a CONACYT program 707986 This work was partially supported by CBH-EUR-GS (ANR-17-EURE-0003).

ACKNOWLEDGMENT

The authors thank the CNRS and Université de Grenoble Alpes for their supports. The NanoBio ICMG (UAR 2607) is acknowledged for providing facilities for mass spectrometry (A. Durand, L. Fort and R. Gueret), elemental analyses (M. Fayolle) and single crystal X-ray diffraction (N. Altounian and Dr. C. Philouze). The theoretical investigations were performed using the computing facilities of the CCIPL (Centre de Calculs Intensifs des Pays de la Loire).

Supporting Information. Experimental details and procedures, Crystal Structures Determinations and Refinements, Absorption

and emission spectroscopies spectra, Computational details, Calculation and NMR spectra. This material is available free of charge via the Internet at http://pubs.acs.org

REFERENCES

(1) Li, T.-Y.; Wu, J.; Wu, Z.-G.; Zheng, Y.-X.; Zuo, J.-L.; Pan, Y. Rational Design of Phosphorescent Iridium(III) Complexes for Emission Color Tunability and Their Applications in OLEDs. *Coord. Chem. Rev.* **2018**, *374*, 55–92. https://doi.org/https://doi.org/10.1016/j.ccr.2018.06.014.

(2) Pashaei, B.; Karimi, S.; Shahroosvand, H.; Abbasi, P.; Pilkington, M.; Bartolotta, A.; Fresta, E.; Fernandez-Cestau, J.; Costa, R. D.; Bonaccorso, F. Polypyridyl Ligands as a Versatile Platform for Solid-State Light-Emitting Devices. *Chem. Soc. Rev.* **2019**, *48* (19), 5033–5139. https://doi.org/10.1039/C8CS00075A.

(3) Costa, R. D.; Ortí, E.; Bolink, H. J.; Graber, S.; Schaffner, S.; Neuburger, M.; Housecroft, C. E.; Constable, E. C. Archetype Cationic Iridium Complexes and Their Use in Solid-State Light-Emitting Electrochemical Cells. *Adv. Funct. Mater.* **2009**, *19* (21), 3456–3463. https://doi.org/10.1002/adfm.200900911.

(4) Meier, S. B.; Tordera, D.; Pertegàs, A.; Roldàn-Carmona, C.; Ortì, E.; Bolink, H. J. Light-Emitting Electrochemical Cells: Recent Progress and Future Prospects. *Mater. Today* **2014**, *17* (5), 217–223. https://doi.org/10.1016/j.mattod.2014.04.029.

(5) Salehi, A.; Fu, X.; Shin, D.-H.; So, F. Recent Advances in OLED Optical Design. *Adv. Funct. Mater.* **2019**, *29* (15), 1808803. https://doi.org/https://doi.org/10.1002/adfm.201808803.

(6) Zhao, J. H.; Hu, Y. X.; Lu, H. Y.; Lü, Y. L.; Li, X. Progress on Benzimidazole-Based Iridium(III) Complexes for Application in Phosphorescent OLEDs. *Org. Electron.* **2017**, *41*, 56–72. https://doi.org/10.1016/j.orgel.2016.11.039.

(7) Choy, W. C. H.; Chan, W. K.; Yuan, Y. Recent Advances in Transition Metal Complexes and Light-Management Engineering in Organic Optoelectronic Devices. *Adv. Mater.* **2014**, *26* (31), 5368–5399. https://doi.org/10.1002/adma.201306133.

(8) Lo, K. K.-W. Luminescent Rhenium(I) and Iridium(III) Polypyridine Complexes as Biological Probes, Imaging Reagents, and Photocytotoxic Agents. *Acc. Chem. Res.* **2015**, *48* (12), 2985–2995. https://doi.org/10.1021/acs.accounts.5b00211.

(9) Yuan, Y. J.; Yu, Z. T.; Chen, D. Q.; Zou, Z. G. Metal-Complex Chromophores for Solar Hydrogen Generation. *Chem. Soc. Rev.* **2017**, *46* (3), 603–631. https://doi.org/10.1039/c6cs00436a.

(10) Prier, C. K.; Rankic, D. a; MacMillan, D. W. C. Visible Light Photoredox Catalysis with Transition Metal Complexes: Applications in Organic Synthesis. *Chem. Rev.* **2013**, *113* (7), 5322–5363. https://doi.org/10.1021/cr300503r.

(11) Shon, J. H.; Teets, T. S. Molecular Photosensitizers in Energy Research and Catalysis: Design Principles and Recent Developments. *ACS Energy Lett.* **2019**, *4* (2), 558–566. https://doi.org/10.1021/acsenergylett.8b02388.

(12) Zhao, Q.; Li, L.; Li, F.; Yu, M.; Liu, Z.; Yi, T.; Huang, C. Aggregation-Induced Phosphorescent Emission (AIPE) of Iridium(Iii) Complexes. *Chem. Commun.* **2008**, *3* (6), 685–687. https://doi.org/10.1039/b712416c.

(13) Solomatina, A. I.; Slobodina, A. D.; Ryabova, E. V; Bolshakova, O. I.; Chelushkin, P. S.; Sarantseva, S. V; Tunik, S. P. Blood-Brain Barrier Penetrating Luminescent Conjugates Based on Cyclometalated Platinum(II) Complexes. *Bioconjug. Chem.* **2020**, *31* (11), 2628–2637. https://doi.org/10.1021/acs.bioconjchem.0c00542.

(14) Flamigni, L.; Barbieri, A.; Sabatini, C.; Ventura, B.; Barigelletti, F. Photochemistry and Photophysics of Coordination Compounds: Iridium. In *Photochemistry and Photophysics of Coordination Compounds II*; 2007; pp 143–203.

(15) Xu, Z.; Tang, B. Z.; Wang, Y.; Ma, D. Recent Advances in High Performance Blue Organic Light-Emitting Diodes Based on Fluorescence Emitters. *J. Mater. Chem. C* **2020**, *8* (8), 2614–2642. https://doi.org/10.1039/C9TC06441A.

(16) Shon, J.-H.; Sittel, S.; Teets, T. S. Synthesis and Characterization of Strong Cyclometalated Iridium Photoreductants for Application in Photocatalytic Aryl Bromide Hydrodebromination. *ACS Catal.* **2019**, *9* (9), 8646–8658. https://doi.org/10.1021/acscatal.9b02759.

(17) Na, H.; Teets, T. S. Highly Luminescent Cyclometalated Iridium Complexes Generated by Nucleophilic Addition to Coordinated Isocyanides. *J. Am. Chem. Soc.* **2018**, *140* (20), 6353–6360. https://doi.org/10.1021/jacs.8b02416.

(18) Lanoë, P.-H.; Tong, C. M.; Harrington, R. W.; Probert, M. R.; Clegg, W.; Williams, J. A. G.; Kozhevnikov, V. N. Ditopic Bis-Terdentate Cyclometallating Ligands and Their Highly Luminescent Dinuclear Iridium(III) Complexes. *Chem. Commun.* **2014**, *50* (52), 6831–6936. https://doi.org/10.1039/c4cc01808g.

(19) Tao, R.; Qiao, J.; Zhang, G.; Duan, L.; Wang, L.; Qiu, Y. Efficient Near-Infrared-Emitting Cationic Iridium Complexes as Dopants for OLEDs with Small Efficiency Roll-Off. *J. Phys. Chem. C* **2012**, *116* (21), 11658–11664. https://doi.org/10.1021/jp301740c.

(20) Sasabe, H.; Takamatsu, J.; Motoyama, T.; Watanabe, S.; Wagenblast, G.; Langer, N.; Molt, O.; Fuchs, E.; Lennartz, C.; Kido, J. High-Efficiency Blue and White Organic Light-Emitting Devices Incorporating a Blue Iridium Carbene Complex. *Adv. Mater.* **2010**, *22* (44), 5003–5007. https://doi.org/10.1002/adma.201002254.

(21) Congrave, D. G.; Hsu, Y.-T.; Batsanov, A. S.; Beeby, A.; Bryce, M. R. Sky-Blue Emitting Bridged Diiridium Complexes: Beneficial Effects of Intramolecular π–π Stacking. *Dalt. Trans.* **2018**, No. 47, 2086–2098. https://doi.org/10.1039/C7DT04201A.

(22) Wang, X.; Wang, S.; Pan, F.; He, L.; Duan, L. Cationic Iridium Complexes with 5-Phenyl-1 H -1,2,4-Triazole Type Cyclometalating Ligands: Toward Blue-Shifted Emission . *Inorg. Chem.* **2019**, *58* (18), 12132–12145. https://doi.org/10.1021/acs.inorgchem.9b01433.

(23) Henwood, A. F.; Pal, A. K.; Cordes, D. B.; Slawin, A. M. Z.; Rees, T. W.; Momblona, C.; Babaei, A.; Pertegás, A.; Ortí, E.; Bolink, H. J.; et al. Blue-Emitting Cationic Iridium(III) Complexes Featuring Pyridylpyrimidine Ligands and Their Use in Sky-Blue Electroluminescent Devices. *J. Mater. Chem. C* **2017**, *5* (37), 9638–9650. https://doi.org/10.1039/c7tc03110f.

(24) He, L.; Lan, Y.; Ma, D.; Song, X.; Duan, L. Fluorine-Free, Highly Efficient, Blue-Green and Sky-Blue-Emitting Cationic Iridium Complexes and Their Use for Efficient Organic Light-Emitting Diodes. *J. Mater. Chem. C* **2018**, *6* (6), 1509–1520. https://doi.org/10.1039/c7tc04747a.

(25) Kozhevnikov, V. N.; Zheng, Y.; Clough, M.; Al-Attar, H. A.; Griffiths, G. C.; Abdullah, K.; Raisys, S.; Jankus, V.; Bryce, M. R.; Monkman, A. P. Cyclometalated Ir(III) Complexes for High-Efficiency Solution-Processable Blue PhOLEDs. *Chem. Mater.* **2013**, *25* (11), 2352–2358. https://doi.org/10.1021/cm4010773.

(26) Bonfiglio, A.; Pallova, L.; César, V.; Gourlaouen, C.; Bellemin-Laponnaz, S.; Daniel, C.; Polo, F.; Mauro, M. Phosphorescent Cationic Heterodinuclear IrIII/MI Complexes (M=CuI, AuI) with a Hybrid Janus-Type N-Heterocyclic Carbene Bridge. *Chem. Eur. J.* **2020**, *26* (51), 11751–11766. https://doi.org/10.1002/chem.202002767.

(27) Caporale, C.; Massi, M. Cyclometalated Iridium(III) Complexes for Life Science. *Coord. Chem. Rev.* **2018**, *363*, 71–91. https://doi.org/10.1016/j.ccr.2018.02.006.

(28) McKenzie, L. K.; Bryant, H. E.; Weinstein, J. A. Transition Metal Complexes as Photosensitisers in One- and Two-Photon Photodynamic Therapy. *Coord. Chem. Rev.* **2019**, *379*, 2–29. https://doi.org/10.1016/j.ccr.2018.03.020.

(29) Henwood, A. F.; Zysman-Colman, E. Luminescent Iridium Complexes Used in Light-Emitting Electrochemical Cells (LEECs). *Top. Curr. Chem.* **2016**, *374* (36). https://doi.org/10.1007/s41061-016-0036-0.

(30) Housecroft, C. E.; C. Constable, E. Over the LEC Rainbow: Colour and Stability Tuning of Cyclometallated Iridium(III) Complexes in Light-Emitting Electrochemical Cells. *Coord. Chem. Rev.* **2017**, *350*, 155–177. https://doi.org/10.1016/j.ccr.2017.06.016.

(31) Rota Martir, D.; Zysman-Colman, E. Supramolecular Iridium(III) Assemblies. *Coord. Chem. Rev.* **2018**, *364*, 86–117. https://doi.org/10.1016/j.ccr.2018.03.016.

(32) Zanoni, K. P. S.; Coppo, R. L.; Amaral, R. C.; Murakami Iha, N. Y. Ir(III) Complexes Designed for Light-Emitting Devices: Beyond the Luminescence Color Array. *Dalt. Trans.* **2015**, *44* (33), 14559–14573. https://doi.org/10.1039/c5dt01644d.

(33) Scattergood, P. A.; Ranieri, A. M.; Charalambou, L.; Comia, A.; Ross, D. A. W.; Rice, C. R.; Hardman, S. J. O.; Heully, J.-L.; Dixon, I. M.; Massi, M.; et al. Unravelling the Mechanism of Excited-State Interligand Energy Transfer and the Engineering of Dual Emission in [Ir(C ∧ N) 2 (N ∧ N)] + Complexes. *Inorg. Chem.* **2020**, *59* (3), 1785–180. https://doi.org/10.1021/acs.inorgchem.9b03003.

(34) Ertl, C. D.; Momblona, C.; Pertegás, A.; Junquera-Hernández, J. M.; La-Placa, M. G.; Prescimone, A.; Ortí, E.; Housecroft, C. E.; Constable, E. C.; Bolink, H. J. Highly Stable Red-Light-Emitting Electrochemical Cells. *J. Am. Chem. Soc.* **2017**, *139* (8), 3237–3248. https://doi.org/10.1021/jacs.6b13311.

(35) Hasan, K.; Bansal, A. K.; Samuel, I. D. W.; Roldán-Carmona, C.; Bolink, H. J.; Zysman-Colman, E. Tuning the Emission of Cationic Iridium (III) Complexes towards the Red through Methoxy Substitution of the Cyclometalating Ligand. *Sci. Rep.* **2015**, *5* (June), 1–16. https://doi.org/10.1038/srep12325.

(36) Wei, X.; Peng, J.; Cheng, J.; Xie, M.; Lu, Z.; Li, C.; Cao, Y. High Performance Polymer Electrophosphorescent Devices with Tert-Butyl Group Modified Iridium Complexes as Emitters. *Adv. Funct. Mater.* **2007**, *17* (16), 3319–3325. https://doi.org/10.1002/adfm.200700359.

(37) Cai, J. X.; Ye, T. L.; Fan, X. F.; Han, C. M.; Xu, H.; Wang, L. L.; Ma, D. G.; Lin, Y.; Yan, P. F. An Effective Strategy for Small Molecular Solution-Processable Iridium(Iii) Complexes with Ambipolar Characteristics: Towards Efficient Electrophosphorescence and Reduced Efficiency Roll-Off. *J. Mater. Chem.* **2011**, *21* (39), 15405–15416. https://doi.org/10.1039/c1jm12114f.

(38) Ouyang, X.; Chen, D.; Zeng, S.; Zhang, X.; Su, S.; Ge, Z. Highly Efficient and Solution-Processed Iridium Complex for Single-Layer Yellow Electrophosphorescent Diodes. *J. Mater. Chem.* **2012**, *22* (43), 23005–23011. https://doi.org/10.1039/c2jm34462a.

(39) Cao, H.; Sun, H.; Yin, Y.; Wen, X.; Shan, G.; Su, Z.; Zhong, R.; Xie, W.; Li, P.; Zhu, D. Iridium(Iii) Complexes Adopting 1,2-Diphenyl-1H-Benzoimidazole Ligands for Highly Efficient Organic Light-Emitting Diodes with Low Efficiency Roll-off and Non-Doped Feature. *J. Mater. Chem. C* **2014**, *2* (12), 2150–2159. https://doi.org/10.1039/c3tc32092h.

(40) Huang, W. S.; Lin, J. T.; Chien, C. H.; Tao, Y. T.; Sun, S. S.; Wen, Y. S. Highly Phosphorescent Bis-Cyclometalated Iridium Complexes Containing Benzoimidazole-Based Ligands. *Chem. Mater.* **2004**, *16* (12), 2480–2488. https://doi.org/10.1021/cm0498943.

(41) Han, L.; Zhang, D.; Zhou, Y.; Yang, Y.; Woo, H. Y.; Bai, F.; Yang, R. Greenish Yellow Organic Light Emitting Devices Based on Novel Iridium Complexes Containing 2-Cyclohexenyl-1-Phenyl-1H-Benzo[d]Imidazole. *Dyes Pigments* **2013**, *99* (3), 1010–1015. https://doi.org/10.1016/j.dyepig.2013.08.011.

(42) Yu, T.; Yang, F.; Chen, X.; Su, W.; Zhao, Y. Synthesis and Characterization of Green-Emitting Ir (III) Complexes Based on a Functionalized Benzimidazole Ligand. *New J. Chem.* **2017**, *41*, 2046–2054. https://doi.org/10.1039/C6NJ03532A.

(43) Jiao, Y.; Li, M.; Wang, N.; Lu, T.; Zhou, L.; Huang, Y.; Lu, Z.; Luo, D.; Pu, X. A Facile Color-Tuning Strategy for Constructing a Library of Ir(III) Complexes with Fine-Tuned Phosphorescence from Bluish Green to Red Using a Synergetic Substituent Effect of –OCH $_3$ and –CN at Only the C-Ring of C^N Ligand. *J. Mater. Chem. C* **2016**, *4* (19), 4269–4277. https://doi.org/10.1039/C6TC00153J.

(44) Mao, H.-T. T.; Zang, C.-X. X.; Shan, G.-G. G.; Sun, H.-Z. Z.; Xie, W.-F. F.; Su, Z.-M. M. Achieving High Performances of Nondoped OLEDs Using Carbazole and Diphenylphosphoryl-Functionalized Ir(III) Complexes as Active Components. *Inorg. Chem.* **2017**, *56* (16), 9979–9987. https://doi.org/10.1021/acs.inorgchem.7b01516.

(45) Shan, G. G.; Li, H. Bin; Mu, Z. C.; Zhu, D. X.; Su, Z. M.; Liao, Y. Synthesis of Cationic Iridium(III) Complexes with High Quantum Yield via Enhancing the Steric Hindrance of Ligands. *J. Organomet. Chem.* **2012**, *702*, 27–35. https://doi.org/10.1016/j.jorganchem.2011.12.020.

(46) Cao, H.; Sun, H.; Shan, G.; Wu, Y.; Su, Z.; Liao, Y. Simultaneous Modification of N-Alkyl Chains on Cyclometalated and Ancillary Ligands of Cationic Iridium (III) Complexes towards e Ffi Cient Piezochromic Luminescence Properties †. *J. Mater. Chem. C* **2015**, 2341–2349. https://doi.org/10.1039/c4tc02879a.

(47) Yarnell, J. E.; De La Torre, P.; Castellano, F. N. Efficient Phosphorescence from Naphthalenebenzimidizole-Coordinated Iridium(III) Chromophores. *Eur. J. Inorg. Chem.* **2017**, No. Iii, 1–9. https://doi.org/10.1002/ejic.201700669.

(48) Zhao, J.-H.; Hu, Y.-X.; Dong, Y.; Xia, X.; Chi, H.-J.; Xiao, G.-Y.; Li, X.; Zhang, D.-Y. Novel Bluish Green Benzimidazole-Based Iridium(III) Complexes for Highly Efficient Phosphorescent Organic Light-Emitting Diodes. *New J. Chem.* **2017**, *41* (5), 1973–1979. https://doi.org/10.1039/C6NJ03634A.

(49) Cao, H. T.; Ding, L.; Yu, J.; Shan, G. G.; Wang, T.; Sun, H. Z.; Gao, Y.; Xie, W. F.; Su, Z. M. Manipulating Phosphorescence Efficiencies of Orange Iridium(III) Complexes through Ancillary Ligand Control. *Dyes Pigments* **2019**, *160* (May 2018), 119–127. https://doi.org/10.1016/j.dyepig.2018.08.001.

(50) Lemonnier, J. F.; Guénée, L.; Beuchat, C.; Wesolowski, T. A.; Mukherjee, P.; Waldeck, D. H.; Gogick, K. A.; Petoud, S.; Piguet, C. Optimizing Sensitization Processes in Dinuclear Luminescent Lanthanide Oligomers: Selection of Rigid Aromatic Spacers. *J. Am. Chem. Soc.* **2011**, *133* (40), 16219–16234. https://doi.org/10.1021/ja206806t.

(51) Shavaleev, N. M.; Eliseeva, S. V.; Scopelliti, R.; Bünzli, J. C. G. Designing Simple Tridentate Ligands for Highly Luminescent Europium Complexes. *Chem. Eur. J.* **2009**, *15* (41), 10790–10802. https://doi.org/10.1002/chem.200901996.

(52) Tatarin, S. V.; Kalle, P.; Taydakov, I. V.; Varaksina, E. A.; Korshunov, V. M.; Bezzubov, S. I. Sterically Hindered Phenanthroimidazole Ligands Drive the Structural Flexibility and Facile Ligand Exchange in Cyclometalated Iridium(Iii) Complexes . *Dalt. Trans.* **2021**, *50* (20), 6889–6900. https://doi.org/10.1039/d1dt00820j.

(53) Bezzubov, S. I.; Kiselev, Y. M.; Churakov, A. V.; Kozyukhin, S. A.; Sadovnikov, A. A.; Grinberg, V. A.; Emets, V. V.; Doljenko, V. D. Iridium(III) 2-Phenylbenzimidazole Complexes: Synthesis, Structure, Optical Properties, and Applications in Dye-Sensitized Solar Cells. *Eur. J. Inorg. Chem.* **2016**, *2016* (3), 347–354. https://doi.org/10.1002/ejic.201501068.

(54) Shavaleev, N. M.; Scopelliti, R.; Gumy, F.; Bünzli, J.-C. G. C. G. Near-Infrared Luminescence of Nine-Coordinate Neodymium Complexes with Benzimidazole-Substituted 8-Hydroxyquinolines. *Inorg. Chem.* **2008**, *47* (19), 9055–9068. https://doi.org/10.1021/ic8010585.

(55) Sprouse, S.; King, K. A.; Spellane, P. J.; Watts, R. J. Photophysical Effects of Metal-Carbon .Sigma. Bonds in Ortho-Metalated Complexes of Iridium(III) and Rhodium(III). *J. Am. Chem. Soc.* **1984**, *106* (22), 6647–6653. https://doi.org/10.1021/ja00334a031.

(56) Congrave, D. G.; Hsu, Y. ting; Batsanov, A. S.; Beeby, A.; Bryce, M. R. Synthesis, Diastereomer Separation, and Optoelectronic and Structural Properties of Dinuclear Cyclometalated Iridium(III) Complexes with Bridging Diarylhydrazide Ligands. *Organometallics* **2017**, *36* (5), 981–993. https://doi.org/10.1021/acs.organomet.6b00887.

(57) Mao, H. T.; Zang, C. X.; Wen, L. L.; Shan, G. G.; Sun, H. Z.; Xie, W. F.; Su, Z. M. Ir(III) Phosphors Modified with Fluorine Atoms in Pyridine-1,2,4-Triazolyl Ligands for Efficient OLEDs Possessing Low-Efficiency Roll-Off. *Organometallics* **2016**, *35* (22), 3870–3877. https://doi.org/10.1021/acs.organomet.6b00753.

(58) Shen, Q. J.; Pang, X.; Zhao, X. R.; Gao, H. Y.; Sun, H. L.; Jin, W. J. Phosphorescent Cocrystals Constructed by 1,4-Diiodotetrafluorobenzene and Polyaromatic Hydrocarbons Based on C-I···π Halogen Bonding and Other Assisting Weak Interactions. *CrystEngComm* **2012**, *14* (15), 5027–5034. https://doi.org/10.1039/c2ce25338k.

(59) Gilday, L. C.; Robinson, S. W.; Barendt, T. A.; Langton, M. J.;

Mullaney, B. R.; Beer, P. D. Halogen Bonding in Supramolecular Chemistry. *Chem. Rev.* **2015**, *115* (15), 7118–7195. https://doi.org/10.1021/cr500674c.

(60) Kinzhalov, M. A.; Eremina, A. A.; Ivanov, D. M.; Novikov, A. S.; Katlenok, E. A.; Balashev, K. P.; Suslonov, V. V. Halogen and Chalcogen Bonding in Dichloromethane Solvate of Cyclometalated Iridium(III) Isocyanide Complex. *Zeitschrift fur Krist. - Cryst. Mater.* **2017**, *232* (12), 797–805. https://doi.org/10.1515/zkri-2017-2065.

(61) Steiner, T. The Hydrogen Bond in the Solid State. *Angew. Chemie - Int. Ed.* **2002**, *41*, 48–76. https://doi.org/10.1109/CDC.2015.7402694.

(62) Costa, R. D.; Ortí, E.; Tordera, D.; Pertegás, A.; Bolink, H. J.; Graber, S.; Housecroft, C. E.; Sachno, L.; Neuburger, M.; Constable, E. C. Stable and Efficient Solid-State Light-Emitting Electrochemical Cells Based on a Series of Hydrophobic Iridium Complexes. *Adv. Energy Mater.* **2011**, *1* (2), 282–290. https://doi.org/10.1002/aenm.201000069.

(63) Lowry, M. S.; Hudson, W. R.; Pascal, R. A.; Bernhard, S. Accelerated Luminophore Discovery through Combinatorial Synthesis. *J. Am. Chem. Soc.* **2004**, *126* (43), 14129–14135. https://doi.org/10.1021/ja047156+.

(64) Lowry, M. S.; Bernhard, S. Synthetically Tailored Excited States: Phosphorescent, Cyclometalated Iridium(III) Complexes and Their Applications. *Chem. Eur. J.* **2006**, *12* (31), 7970–7977.

(65) Turro, N. J.; Ramamurthy, V.; J. C. Scaiano. *Modern Molecular Photochemistry of Organic Molecules*; 2010.

(66) Hasebe, N.; Deguchi, Y.; Murayama, S.; Yoshihara, T.; Horiuchi, H.; Okutsu, T.; Tobita, S. Phosphorescence Quenching of Neutral and Cationic Iridium(III) Complexes by Molecular Oxygen and Aromatic Electron Acceptors. *J. Photochem. Photobiol. A Chem.* **2016**, *324*, 134–144. https://doi.org/10.1016/j.jphotochem.2016.03.008.

(67) Djurovich, P. I.; Murphy, D.; Thompson, M. E.; Hernandez, B.; Gao, R.; Hunt, P. L.; Selke, M. Cyclometalated Iridium and Platinum Complexes as Singlet Oxygen Photosensitizers: Quantum Yields, Quenching Rates and Correlation with Electronic Structures. *Dalt. Trans.* **2007**, No. 34, 3763–3770.

(68) McKenzie, L. K.; Sazanovich, I. V.; Baggaley, E.; Bonneau, M.; Guerchais, V.; Williams, J. A. G.; Weinstein, J. A.; Bryant, H. E. Metal Complexes for Two-Photon Photodynamic Therapy: A Cyclometallated Iridium Complex Induces Two-Photon Photosensitization of Cancer Cells under Near-IR Light. *Chem. Eur. J.* **2017**, *23* (2), 234–238. https://doi.org/10.1002/chem.201604792.

(69) Montalti, M.; Credi, A.; Prodi, L.; Gandolfi, M. T. Solvent Properties. In *Handbook of Photochemistry*; Taylor & Francis Group, 2006; pp 535–561. https://doi.org/10.1201/9781420015195.

(70) Costa, R. D.; Monti, F.; Accorsi, G.; Barbieri, A.; Bolink, H. J.; Ortí, E.; Armaroli, N. Photophysical Properties of Charged Cyclometalated Ir(III) Complexes: A Joint Theoretical and Experimental Study. *Inorg. Chem.* **2011**, *50* (15), 7229–7238. https://doi.org/10.1021/ic200820t.

(71) Shavaleev, N. M.; Scopelliti, R.; Grätzel, M.; Nazeeruddin, M. K.; Pertegás, A.; Roldán-Carmona, C.; Tordera, D.; Bolink, H. J. Pulsed-Current versus Constant-Voltage Light-Emitting Electrochemical Cells with Trifluoromethyl-Substituted Cationic Iridium(Iii) Complexes. *J. Mater. Chem. C* **2013**, *1* (11), 2241–2248. https://doi.org/10.1039/c3tc00808h.

(72) Whittle, C. E.; Weinstein, J. A.; George, M. W.; Schanze, K. S. Photophysics of Diimine Platinum(II) Bis-Acetylide Complexes. *Inorg. Chem.* **2001**, *40* (16), 4053–4062. https://doi.org/10.1021/ic0102182.

(73) Pomestchenko, I. E.; Castellano, F. N. Solvent Switching between Charge Transfer and Intraligand Excited States in a Multichromophoric Platinum(II) Complex. *J. Phys. Chem. A* **2004**, *108* (16), 3485–3492. https://doi.org/10.1021/jp049641x.

(74) Lees, A. J. The Luminescence Rigidochromic Effect Exhibited by Organometailic Complexes: Rationale and Applications. *Comments Inorg. Chem. A J. Crit. Discuss. Curr. Lit.* **1995**, *17* (6), 319–346. https://doi.org/10.1080/02603599508032711.

(75) Lai, P. N.; Brysacz, C. H.; Alam, M. K.; Ayoub, N. A.; Gray, T. G.; Bao, J.; Teets, T. S. Highly Efficient Red-Emitting Bis-Cyclometalated Iridium Complexes. *J. Am. Chem. Soc.* **2018**, *140* (32), 10198–10207. https://doi.org/10.1021/jacs.8b04841.

(76) Tamayo, A. B.; Garon, S.; Sajoto, T.; Djurovich, P. I.; Tsyba, I. M.; Bau, R.; Thompson, M. E. Cationic Bis-Cyclometalated Iridium(III) Diimine Complexes and Their Use in Efficient Blue, Green, and Red Electroluminescent Devices. *Inorg. Chem.* **2005**, *44* (24), 8723–8732. https://doi.org/10.1021/ic050970t.

(77) Frisch, M. J.; Trucks, G. W.; Schlegel, H. B.; Scuseria, G. E.; Robb, M. A.; Cheeseman, J. R.; Scalmani, G.; Barone, V.; Petersson, G. A.; Nakatsuji, H.; Li, X.; Caricato, M.; Marenich, A. V.; Bloino, J.; Janesko, B. G.; Gomperts, R.; Mennucci, B.; Hratch, D. J. Gaussian 16, Revision B.01. Gaussian Inc.: Wallingford CT 2016.

(78) Vazart, F.; Latouche, C. Validation of a Computational Protocol to Simulate near IR Phosphorescence Spectra for Ru(II) and Ir(III) Metal Complexes. *Theor. Chem. Acc.* **2015**, *134* (12), 144. https://doi.org/10.1007/s00214-015-1737-0.

(79) Latouche, C.; Palazzetti, F.; Skouteris, D.; Barone, V. High-Accuracy Vibrational Computations for Transition-Metal Complexes Including Anharmonic Corrections: Ferrocene, Ruthenocene, and Osmocene as Test Cases. *J. Chem. Theory Comput.* **2014**, *10* (10), 4565–4573. https://doi.org/10.1021/ct5006246.

(80) Latouche, C.; Baiardi, A.; Barone, V. Virtual Eyes Designed for Quantitative Spectroscopy of Inorganic Complexes: Vibronic Signatures in the Phosphorescence Spectra of Terpyridine Derivatives. *J. Phys. Chem. B* **2015**, *119* (24), 7253–7257. https://doi.org/10.1021/jp510589u.

(81) Latouche, C.; Skouteris, D.; Palazzetti, F.; Barone, V. TD-DFT Benchmark on Inorganic Pt(II) and Ir(III) Complexes. *J. Chem. Theory Comput.* **2015**, *11* (7), 3281–3289. https://doi.org/10.1021/acs.jctc.5b00257.

(82) Perdew, J. P.; Burke, K.; Wang, Y. Generalized Gradient Approximation for the Exchange-Correlation Hole of a Many-Electron System. *Phys. Rev. B* **1996**, *54* (23), 16533–16539. https://doi.org/10.1103/PhysRevB.54.16533.

(83) Perdew, J. P. Density-Functional Approximation for the Correlation Energy of the Inhomogeneous Electron Gas. *Phys. Rev. B* **1986**, *33* (12), 8822–8824. https://doi.org/10.1103/PhysRevB.33.8822.

(84) Becke, A. D. Density-functional Thermochemistry. III. The Role of Exact Exchange. *J. Chem. Phys.* **1993**, *98* (7), 5648–5652. https://doi.org/10.1063/1.464913.

(85) Dunning, T. H.; Hay, P. J. Gaussian Basis Sets for Molecular Calculations BT - Methods of Electronic Structure Theory; Schaefer, H. F., Ed.; Springer US: Boston, MA, 1977; pp 1–27. https://doi.org/10.1007/978-1-4757-0887-5_1.

(86) Wadt, W. R.; Hay, P. J. Ab Initio Effective Core Potentials for Molecular Calculations. Potentials for Main Group Elements Na to Bi. *J. Chem. Phys.* **1985**, *82* (1), 284–298. https://doi.org/10.1063/1.448800.

(87) Hay, P. J.; Wadt, W. R. Ab Initio Effective Core Potentials for Molecular Calculations. Potentials for K to Au Including the Outermost Core Orbitals. *J. Chem. Phys.* **1985**, *82* (1), 299–310. https://doi.org/10.1063/1.448975.

(88) Hay, P. J.; Wadt, W. R. Ab Initio Effective Core Potentials for Molecular Calculations. Potentials for the Transition Metal Atoms Sc to Hg. *J. Chem. Phys.* **1985**, *82* (1), 270–283. https://doi.org/10.1063/1.448799.

(89) Schira, R.; Latouche, C. DFT vs. TDDFT vs. TDA to Simulate Phosphorescence Spectra of Pt- and Ir-Based Complexes. *Dalt. Trans.* **2021**, *50* (2), 746–753. https://doi.org/10.1039/D0DT03614E.

(90) Benedetta Mennucci, R. C. *Continuum Solvation Models in Chemical Physics: From Theory to Applications*, Wiley.; Wiley, 2008. https://doi.org/10.1002/9780470515235.

(91) Mennucci, B.; Tomasi, J.; Cammi, R.; Cheeseman, J. R.; Frisch, M. J.; Devlin, F. J.; Gabriel, S.; Stephens, P. J. Polarizable Continuum Model (PCM) Calculations of Solvent Effects on Optical Rotations of Chiral Molecules. *J. Phys. Chem. A* **2002**, *106* (25), 6102–6113. https://doi.org/10.1021/jp020124t.

(92) Bloino, J.; Biczysko, M.; Santoro, F.; Barone, V. General

Approach to Compute Vibrationally Resolved One-Photon Electronic Spectra. *J. Chem. Theory Comput.* **2010**, *6* (4), 1256–1274. https://doi.org/10.1021/ct9006772.

(93) Licari, D.; Baiardi, A.; Biczysko, M.; Egidi, F.; Latouche, C.; Barone, V. Implementation of a Graphical User Interface for the Virtual Multifrequency Spectrometer: The VMS-Draw Tool. *J. Comput. Chem.* **2015**, *36* (5), 321–334. https://doi.org/https://doi.org/10.1002/jcc.23785.

(94) Barone, V. The Virtual Multifrequency Spectrometer: A New Paradigm for Spectroscopy. *WIREs Comput. Mol. Sci.* **2016**, *6* (2), 86–110. https://doi.org/https://doi.org/10.1002/wcms.1238.

(95) Dennington, R.; Keith, T. A.; Millam, J. M. GaussView Version 6. 2019.

(96) Duisenberg, A. J. M.; Kroon-Batenburg, L. M. J.; Schreurs, A. M. M. An Intensity Evaluation Method: EVAL-14. *J. Appl. Crystallogr.* **2003**, *36* (2), 220–229. https://doi.org/10.1107/S0021889802022628.

(97) Palatinus, L.; Chapuis, G. SUPERFLIP - A Computer Program for the Solution of Crystal Structures by Charge Flipping in Arbitrary Dimensions. *J. Appl. Crystallogr.* **2007**, *40* (4), 786–790. https://doi.org/10.1107/S0021889807029238.

(98) Sheldrick, G. M. Crystal Structure Refinement with SHELXL. *Acta Crystallogr. Sect. C Struct. Chem.* **2015**, *71* (Md), 3–8. https://doi.org/10.1107/S2053229614024218.

(99) Dolomanov, O. V.; Bourhis, L. J.; Gildea, R. J.; Howard, J. A. K. K.; Puschmann, H. OLEX2: A Complete Structure Solution, Refinement and Analysis Program. *J. Appl. Crystallogr.* **2009**, *42* (2), 339–341. https://doi.org/10.1107/S0021889808042726.

(100) Join, B.; Möller, K.; Ziebart, C.; Schröder, K.; Gördes, D.; Thurow, K.; Spannenberg, A.; Junge, K.; Beller, M. Selective Iron-Catalyzed Oxidation of Benzylic and Allylic Alcohols. *Adv. Synth. Catal.* **2011**, *353* (16), 3023–3030. https://doi.org/10.1002/adsc.201100210.

(101) Huang, J.; Li, G. X.; Yang, G. F.; Fu, D. Q.; Nie, X. K.; Cui, X.; Zhao, J. Z.; Tang, Z. Catalytic Asymmetric Synthesis OfN-Substituted Tetrahydroquinoxalinesviaregioselective Heyns Rearrangement and Stereoselective Transfer Hydrogenation in One Pot. *Chem. Sci.* **2021**, *12* (13), 4789–4793. https://doi.org/10.1039/d0sc06264b.

(102) Sun, X.; Lv, X.-H.; Ye, L.-M.; Hu, Y.; Chen, Y.-Y.; Zhang, X.-J.; Yan, M. Synthesis of Benzimidazoles via Iridium-Catalyzed Acceptorless Dehydrogenative Coupling. *Org. Biomol. Chem.* **2015**, *13* (27), 7381–7383. https://doi.org/10.1039/C5OB00904A.

(103) Bose, A.; Maiti, S.; Sau, S.; Mal, P. An Intramolecular C(Sp3)-H Imination Using PhI-m CPBA. *Chem. Commun.* **2019**, *55* (14), 2066–2069. https://doi.org/10.1039/c8cc09100e.

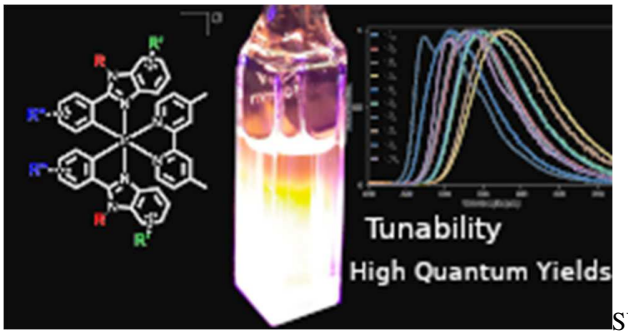

SYNOPSIS TOC: We investigate a new family of cationic iridium(III) complexes featuring 2-phenylbenzimidazole cyclometallating ligand and 4,4'-dimethyl-2,2'-bipyridine ancillary ligand. The complexes have been fully characterized by ^{1}H and ^{13}C NMR spectroscopy, HRMS. In addition, we have performed a study of their emission properties supported by accurate theoretical calculations.

---

[i] Bruker (2004). *SADABS.* Bruker AXS Inc., Madison, Wisconsin, USA.
[ii] Bruker (2005). *XPREP.* Bruker AXS Inc., Madison, Wisconsin, USA.